Synthetic Aperture Radar Image Statistical Modeling

Part Two—Spatial correlation models and simulation

DONG-XIAO YUE, FENG XU, ALEJANDRO C. FRERY, AND YA-QIU JIN

xxxxx

Following on the first part of our review of synthetic aperture radar (SAR) image statistical modeling [1], which concerns single-pixel statistical models, this article extends our discussion to spatial correlation analysis, focusing on SAR spatial correlation models and SAR clutter simulation methods. Two types of spatial correlation models, the product model and the coherent scatterer model, are summarized: the first considers correlation characteristics from the image itself while the second analyzes spatial correlation stemming from the underlying scatterer and the physical imaging process. In addition, we review four spatially correlated clutter simulation methods based on two classical distributions (K and G^0): a product model-based method, an inverse transform method (ITM)-based approach, a coherent scatterer model-based technique, and the generalized Gaussian coherent scatterer (GGCS) approach. We discuss the advantages and disadvantages of these models and methods and provide references for further research into the statistical modeling of SAR images.

BACKGROUND

The statistical modeling of SAR images has formed one of the essential research subjects focused on SAR image interpretation. An in-depth study of the statistical characteristics of SAR images can provide strong support for SAR image information extraction and interpretation algorithm verification, and it is the theoretical basis for applications such as target detection and recognition. At present, most statistical modeling of SAR images considers the single-pixel statistical model, which was summarized from different perspectives in [1]. However, single-pixel models cannot solely represent the texture characteristics of an image, leaving them far from sufficient for mining SAR image information [2]. Two-pixel statistical models, such as the power spectrum and the autocorrelation function, can further characterize the texture information of the spatial variation in SAR imagery, which we call *spatially correlated statistical modeling*. As the second part of a treatment of SAR image statistical modeling, this article continues to review the spatial correlation analysis of SAR images built on the single-pixel statistical model [1].

The spatial correlation models of SAR images also have different analysis methods through the development of single-pixel probability distribution models. The correlation analysis of SAR images was first discussed by Jakeman and Pusey [3] when they proposed K-distributed sea clutter. They gave the expressions of the high-order moment and the autocorrelation function of the radar cross-section (RCS). They also provided the relationship between the autocorrelation function of the RCS and the number of scatterers, with which they defined the concept of the number of equivalent scatterers. Subsequently, [4] and [5] derived the influence of the number of scatterers that obey the negative binomial distribution on the spatial correlation.

A large number of previous models of non-Gaussian clutter focus on the statistical analysis of the correlated K-distributed clutter, and the correlation analysis is mainly based on the development of a coherent scatterer model described by a random walk process. Oliver et al. considered

Digital Object Identifier 10.1109/MGRS.2020.3027609
Date of current version: 17 November 2020

the influence of the imaging system and proposed multiple surface cross-section models for describing the *K*-distributed correlated clutter [6]–[9]. The *K*-distributed correlated clutter is modeled as the output of the correlated gamma-distributed RCS after the imaging system. It mainly includes two models for simulating the RCS.

One is an accurate representation based on gamma–Lorentzian intensity fluctuations [6], [7], which describe the gamma-distributed RCS as the solution of the Fokker–Planck equation (a continuous form of the birth–death-migration ratio equation [10], [11]) that can be obtained by numerical simulation using stochastic differential equations. This model can accurately express the higher-order statistical characteristics of the correlated *K*-distributed clutter. Its limitation is that it can represent only the exponential correlation function and is suitable for 1D situations alone.

The other representation is an approximate model based on a linear filter [8]. It uses an uncorrelated gamma-distributed RCS to obtain a correlated gamma-distributed RCS through a linear filter. The uncorrelated gamma distribution can be regarded as a Gaussian random walk process. This model is widely employed since it can describe arbitrary correlation functions and represent 2D clutter images. The disadvantage of this method is that it can accurately represent only second-order correlation moments, with possible deviations for higher-order moments. Also, it is applicable only to the case where the order of the gamma distribution is a semi-integer. The author of [12] discussed a method for simulating correlated clutter images with an arbitrary power spectrum based on an approximate model. To overcome the shortcoming that the approximate model can describe only the semi-integer-order gamma distribution, more theoretical models and simulation methods of correlated gamma distribution have gradually been proposed [13], [14], such as the memoryless nonlinear transform (MNLT) technique [13].

To characterize non-Gaussian clutter with more general models, Conte et al. [15]–[18] proposed a complex spherical invariant random process (SIRP) to model SAR complex clutter images. The advantage of the SIRP process is that, as with the Gaussian distribution, it is completely determined by the mean and the covariance function. This process has linear transformation properties that are similar to Gaussian variables, which facilitates the selection of correlated structures. This model ensures that the joint probability density function (PDF) of the real and imaginary components of complex clutter is circularly symmetric; that is, the phase obeys a uniform distribution. The autocorrelation structure and cross-correlation structure of the real and imaginary components are flexible and can be stipulated according to a specific physical scene. The closed-form, higher-order probability distribution expression of this model is available, and it can reduce to the simplest case, where the amplitude obeys the Rayleigh distribution. The SIRP is able to represent the *K* distribution, which is expressed as the product of a Rayleigh-distributed variable and a gamma-distributed variable, and the Weibull distribution by constraining specific parameters. The disadvantage of this model is that it can represent only amplitude images that obey the distribution of mixed Rayleigh laws. As an example, it cannot express the lognormal distribution.

Based on the preceding research, Conte et al. [17] further proposed a composite process to model radar clutter as a product of the complex SIRP process and independent nonnegative random variables. The approach can be considered as the modulation of the SIRP process, and its correlation characteristics are introduced by the complex SIRP process. Correlation functions of clutter can also be expressed as the product of the correlation functions of the complex Gaussian process and a nonnegative random process. The nature of the model is consistent with the product model proposed by Ward [19] and the correlation analysis by Ulaby et al. [20], both of whom model the speckle as multiplicative noise. The product model has also been one of the most popular ones in the statistical representation of SAR images. The authors of [17] provided simulation methods for correlated *K*-distributed clutter and correlated Weibull-distributed clutter based on the exogenous model [15].

This article analyzes the existing spatial correlation models from two perspectives: the product model [19] and the coherent scatterer model [6]. The product model describes the SAR image observations as the product of the RCS component and the speckle component. The correlation is the product of the correlation function of the RCS and the speckle. The product model is simple and easy to implement and analyze, but it is difficult to establish a corresponding relationship with the physical scattering process. The coherent scatterer model, also known as the *discrete scatterer model*, is a relatively complex statistical representation based on physical scattering processes. It analyzes the relevant characteristics of an SAR image based on factors such as the number of scatterers, the RCS, and the imaging impulse response. This method has strong physical interpretability, which is valuable for the interpretation of high-resolution SAR images.

In addition, as an important application of SAR image statistical modeling, this article reviews the main correlated clutter simulation methods based on the single-pixel statistical models along with their correlation analysis. Clutter simulation is a forward process for modeling SAR images. It is an important tool for validating whether the properties of SAR images have been well understood. It has significant applications for despeckling [21], [22], target detection and recognition [23], [24], interpretation algorithm verification [25], [26], system design verification, and accuracy evaluation [27], [28]. It is a vital way to describe SAR clutter based on the statistical characteristics of observed data at a single-pixel and observed data at a single-pixel and the correlation structures of these data [29], [30].

The *K* distribution [4] has been the most widely used statistical distribution in the study of non-Gaussian clutter

models. It can be used to describe sea, forest, and other scenarios, but it cannot define extremely inhomogeneous regions. The G^0 distribution [31] is able to depict homogeneous, inhomogeneous, and extremely inhomogeneous scenes. Therefore, this article reviews four main correlated clutter simulation methods based on these two classical distribution models: the simulation of correlated *K*-distributed clutter based on the product model [2], the simulation of the correlated G^0-distributed clutter [30] based on the ITM, the simulation of the correlated *K*-distributed clutter based on the coherent scatterer model [32], and the simulation of correlated clutter based on the GGCS model.

SPATIAL CORRELATION MODELS

In [1], we investigate the development of more than 20 single-pixel statistical distributions based on the Rayleigh speckle model, the product model, the non-Rayleigh speckle model, the generalized central limit theorem model, the incoherent scatterer sum model, the single empirical distribution model, and the finite mixture statistical model. The single-pixel statistical model is not sufficient to completely describe SAR clutter, as it does not convey the spatial information of the image. Therefore, the two-pixel statistical characteristics (the power spectrum and the correlation function) of the SAR image need further study. This section summarizes the commonly used spatial correlation models of SAR images.

As shown in Figure 1, the correlation analysis of SAR images is mainly divided into two approaches, which include the following:

1) *Correlation analysis based on the product model [20]*: The main idea is to consider the scattered echo as the product of the speckle component and the RCS component. The correlation function of the scattered echo can also be regarded as the product of the correlation functions of the speckle and the RCS components. In this way, first, the correlation functions of these two components are separately modeled, and then the product model is used to derive the correlation information of an SAR image.

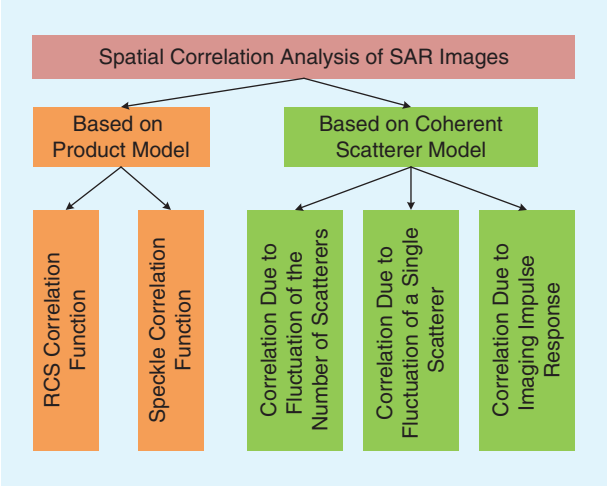

FIGURE 1. A spatial correlation analysis of SAR images.

2) *Correlation analysis based on the coherent scatterer model [4], [7]*: The purpose here is to model the scattered field of an SAR image as a random walk and to analyze the correlation information introduced in the scattering process. Research shows that the number of scatterers, the fluctuation of the scattered field of a single scatterer, and the imaging impulse response function are the main factors affecting the correlation of the observed intensity.

This section will introduce these methods one by one. Figure 2 outlines the main context of the spatial correlation analysis introduced in this section, which is detailed in the following.

CORRELATION ANALYSIS BASED ON THE PRODUCT MODEL

The product model was proposed by Ward in 1981 [19]. It represents the image data as the product of the RCS and the uncorrelated speckle noise. The speckle is caused by the coherent imaging process, and the RCS is characterized by the deterministic information of the scene, such as the texture data. The product model is simple but able to describe the characteristics of nonuniform regions that have texture. It has been the most popular model in the field of statistical modeling of SAR images [2].

Ulaby et al. [20] analyzed the correlation property of observed SAR images based on the product model, which represented the SAR image observations as the product of the average intensity, the normalized texture, and an uncorrelated speckle component, as documented in Figure 2. To be consistent with the traditional product model, the product of the average intensity and the normalized texture component is regarded as the RCS. For the 2D SAR intensity image I, the product model [19], [20] at a certain pixel (x, y) can be expressed as

$$I(x,y)=\sigma(x,y)\,n(x,y), \tag{1}$$

where $I(x,y)$ is a random variable with average intensity μ_I and variance s_I^2, $\sigma(x,y)$ is the RCS with mean μ_σ and variance s_σ^2, and $n(x,y)$ is the normalized speckle random variable with mean $\mu_n=1$ and variance $s_n^2=1/N$, where N is the number of looks.

The autocorrelation function and autocorrelation coefficient of SAR intensity image I are, respectively,

$$R_I(\Delta x,\Delta y;N)=<I\ (x,y)\,I\ (x+\Delta x,y+\Delta y)>, \tag{2}$$

$$\rho_I(\Delta x,\Delta y)=\frac{R_I(\Delta x,\Delta y)-\mu_I^2}{s_I^2}, \tag{3}$$

where $\langle\cdot\rangle$ denotes taking the expectation, Δx and Δy indicate, respectively, the distances in the azimuth and range directions. Assuming that $\sigma(x,y)$ and $n(x,y)$ are independent random variables, the autocorrelation function of I is, according to this model [20],

$$R_I(\Delta x,\Delta y;N)=R_\sigma(\Delta x,\Delta y)\,R_n(\Delta x,\Delta y;N), \tag{4}$$

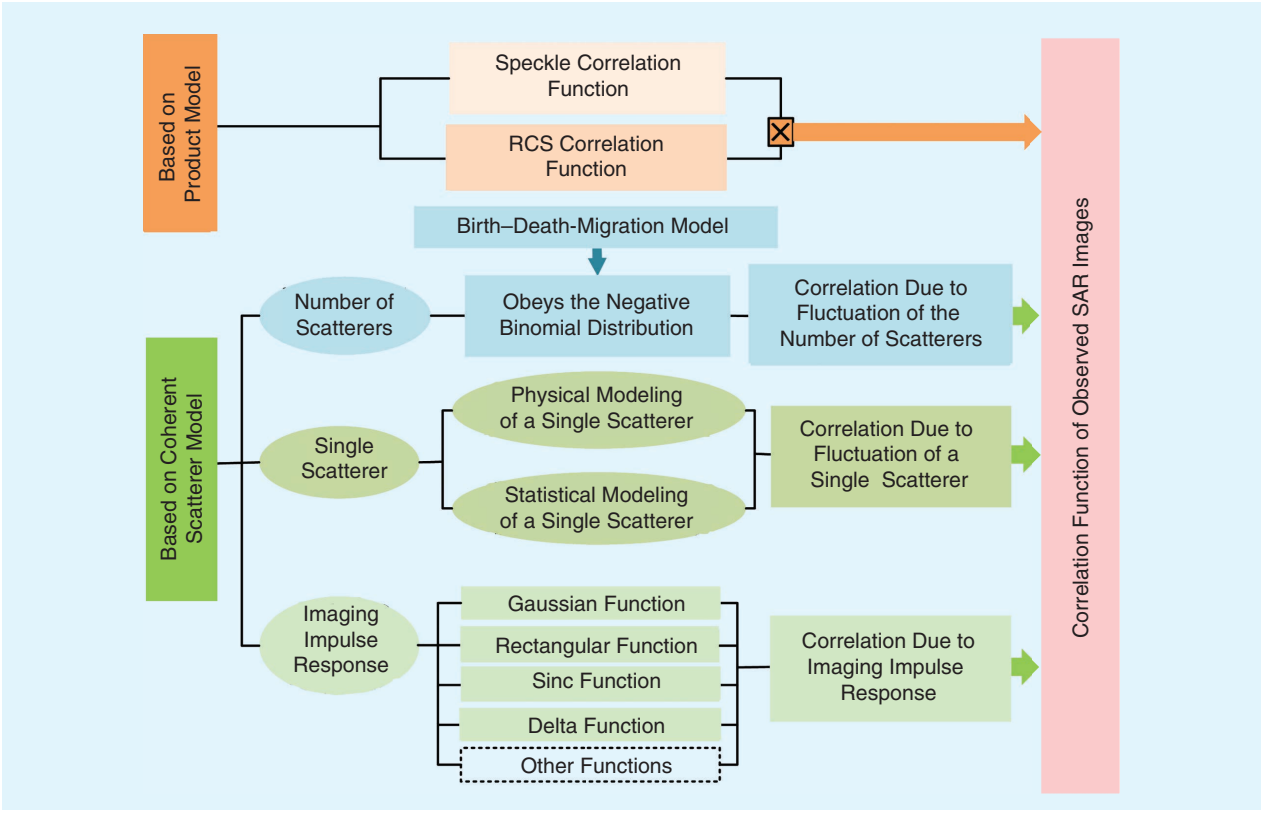

FIGURE 2. The context of spatial correlation analysis.

where $R_\sigma(\Delta x, \Delta y)$ is the autocorrelation function of the RCS $\sigma(x, y)$, and $R_n(\Delta x, \Delta y; N)$ represents the autocorrelation function of the speckle $n(x, y)$. It can be seen that the correlation functions also satisfy the product relationship, and R_I is determined by the autocorrelation functions of the speckle R_n and the RCS R_σ.

The speckle is white noise, and there is no correlation in itself. The correlation shown in the SAR image is introduced during the imaging focus process. The authors of [20] gave the autocorrelation function of the speckle of the intensity image

$$R_n(\Delta x, \Delta y; N) = \frac{1}{N}\text{sinc}^2\left(\frac{\Delta x}{r_x}\right)\text{sinc}^2\left(\frac{\Delta y}{r_y}\right) + 1, \tag{5}$$

where r_x and r_y are the corresponding spatial resolution in the azimuth and range directions of the sensor. The corresponding autocovariance is

$$\begin{aligned} C_n(\Delta x, \Delta y; N) &= R_n(\Delta x, \Delta y; N) - \mu_n^2 \\ &= \frac{1}{N}\text{sinc}^2\left(\frac{\Delta x}{r_x}\right)\text{sinc}^2\left(\frac{\Delta y}{r_y}\right). \end{aligned} \tag{6}$$

In [20], the authors pointed out that, if the pixel interval (or the sampling interval) is greater than the spatial resolution, the correlation of neighboring pixels can be ignored. Generally, if the pixel distance is 0.5–1 spatial-resolution cell (that is, oversampling), two adjacent pixels are correlated, and two pixels with an interval greater than one pixel are uncorrelated.

Similar to (3), the autocorrelation function of the RCS can be written as

$$R_\sigma(\Delta x, \Delta y) = s_\sigma^2 \rho_\sigma(\Delta x, \Delta y) + \mu_\sigma^2, \tag{7}$$

where $\rho_\sigma(\Delta x, \Delta y)$ is the autocorrelation coefficient of the RCS. Substituting (3), (7), and $\mu_\sigma^2 = \mu_I^2$ into (4) obtains

$$\rho_\sigma(\Delta x, \Delta y) = \frac{1}{s_\sigma^2}\left[\frac{\rho_I(\Delta x, \Delta y)s_I^2 + \mu_I^2}{R_n(\Delta x, \Delta y)} - \mu_I^2\right]. \tag{8}$$

Usually, the negative exponential correlation function is adopted [2], [32]:

$$\rho_\sigma(\Delta x, \Delta y) = \exp\left[-\frac{2|\Delta x|}{\ell_x} - \frac{2|\Delta y|}{\ell_y}\right], \tag{9}$$

where x and y are the azimuth and the range, respectively, and ℓ_x and ℓ_y are the corresponding $1/e$ correlation lengths.

CORRELATION ANALYSIS BASED ON THE COHERENT SCATTERER MODEL

This section introduces correlation analysis based on the coherent scatterer model, as given in Figure 2. The physically coherent scatterer model is discussed, followed by the influence of the number of scatterers, the amplitude fluctuation of a single scatterer, and the imaging impulse response function on the correlation structure of an SAR image.

COHERENT SCATTERER MODEL

The coherent scatterer model describes the speckle phenomenon that results from the summation of a large number of complex components with independent phases [2], [10]. Figure 3 presents a sketch of the 2D coherent scatterer model. As shown in Figure 3, the scattering process is divided into two steps: the coherent scatterer model and the scattering imaging process. The coherent scatterer model characterizes the process of the coherent summation of multiple scatterers to obtain a scattered field. The first layer, at the left in Figure 3, illustrates the random distributed scatterers (indicated by black dots) in a 2D plane (the xy-plane), where each square denotes a resolution cell. The scattered field of the second layer (designated by red asterisks) is obtained by the coherent summation of the scatterers of the first layer in each resolution cell. The third layer denotes the observations (specified by blue diamonds), i.e., the pixel values of the image, which are obtained by the scattered field through the imaging system.

The mathematical model of the scattering process is described on the right side of Figure 3. The scattered field $E(x,y)$ at (x,y) can be regarded as the summation of N scatterers in a resolution cell [2], [4]:

$$E(x,y) = A(x,y)e^{j\theta(x,y)} = \sum_{i=1}^{N} a_i e^{j\phi_i} = \sum_{i=1}^{N} a_{x,y,i}, \tag{10}$$

where $A(x,y)$ and $\theta(x,y)$ are the amplitude and the phase of the scattered field at position (x,y), respectively, and $a_{x,y,i}$, a_i and ϕ_i are the complex scattered value and the scattered amplitude and phase of the ith $(1 \le i \le N)$ scatterer at (x,y), respectively.

The RCS $\sigma(x,y)$ at (x,y) is defined as

$$\sigma(x,y) = E(x,y)\cdot E^*(x,y) = A^2(x,y). \tag{11}$$

The correlation functions of the 2D scattered field E and the RCS σ at two points (x,y) and $(x+\Delta x, y+\Delta y)$ are

$$\rho^{(1)}(\Delta x,\Delta y) = \frac{\langle E(x,y)E^*(x+\Delta x,y+\Delta y)\rangle}{\langle\sigma\rangle}, \tag{12}$$

$$\rho^{(2)}(\Delta x,\Delta y) = \frac{\langle \sigma(x,y)\sigma^*(x+\Delta x,y+\Delta y)\rangle}{\langle\sigma\rangle^2}, \tag{13}$$

where $\langle\sigma\rangle = \langle A(x,y)A^*(x,y)\rangle$ and the brackets denote the expected value. If the number of scatterers is a constant N, (12) and (13) can be written as [5]

$$\rho^{(1)}(\Delta x,\Delta y) = \langle A(x,y)A^*(x+\Delta x,y+\Delta y)\rangle \times \frac{\langle \exp\{i[\theta(x,y)-\theta(x+\Delta x,y+\Delta y)]\}\rangle}{\langle\sigma\rangle}, \tag{14}$$

$$\begin{aligned}\rho^{(2)}(\Delta x,\Delta y) &= \left(1-\frac{1}{N}\right)\left(1+\left|\rho^{(1)}(\Delta x,\Delta y)\right|^2\right) \\ &\quad + \frac{\langle A^2(x,y)A^2(x+\Delta x,y+\Delta y)\rangle}{N\langle A^2(x,y)\rangle\langle A^2(x+\Delta x,y+\Delta y)\rangle} \\ &= \left(1-\frac{1}{N}\right)\left(1+\left|\rho^{(1)}(\Delta x,\Delta y)\right|^2\right) \\ &\quad + \frac{\langle \sigma(x,y)\sigma^*(x+\Delta x,y+\Delta y)\rangle}{N\langle\sigma^2\rangle}.\end{aligned} \tag{15}$$

If N is large, (15) can be simplified and becomes

$$\rho^{(2)}(\Delta x,\Delta y) = \left(1-\frac{1}{N}\right)\left(1+\left|\rho^{(1)}(\Delta x,\Delta y)\right|^2\right). \tag{16}$$

Considering the impulse response of the imaging system, the single-look complex image at position (x,y) can be modeled as [6]–[9]

$$\varepsilon(x,y) = B\int_{-\infty}^{\infty}\int_{-\infty}^{\infty} dx_1\,dy_1 A(x_1,y_1)e^{j\theta(x_1,y_1)}h(x_1,y_1), \tag{17}$$

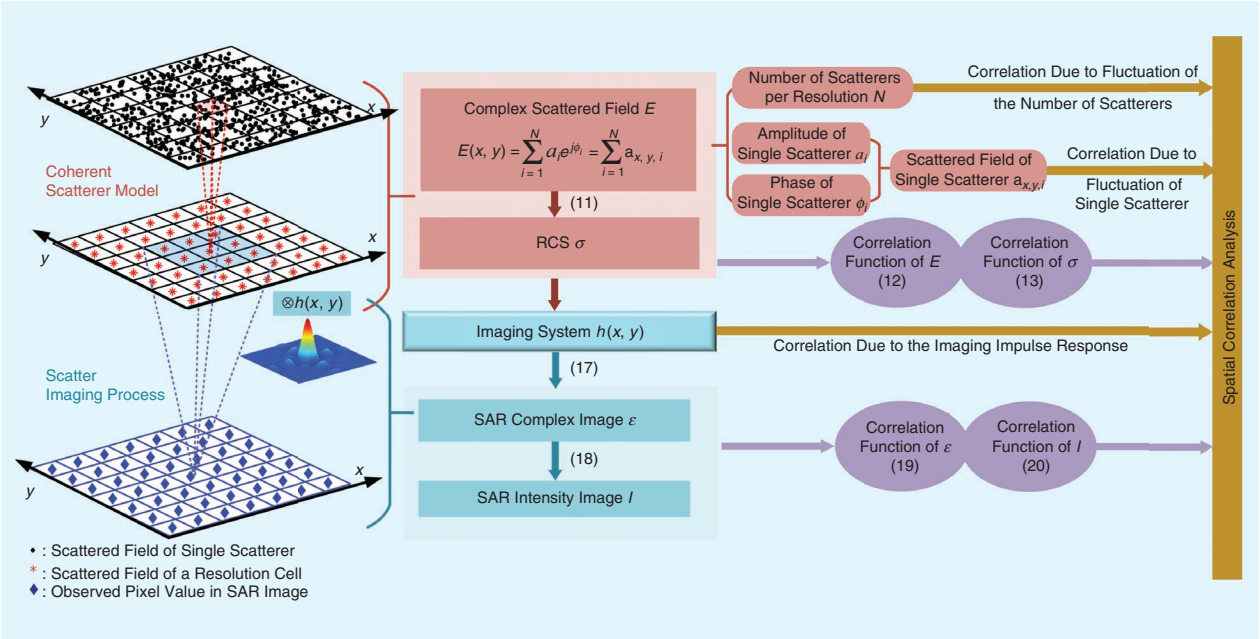

FIGURE 3. A spatial correlation analysis based on the coherent scatterer model.

where B is a constant that denotes the gain of the radar equation and $h(x_1, y_1)$ is the impulse response of imaging system. The intensity I of the observed image is [6]–[9]

$$I(x, y) = |\varepsilon(x, y)|^2. \tag{18}$$

The 2D correlation function of the single-look complex image ε and the image intensity I are defined as

$$g^{(1)}(\Delta x, \Delta y) = \frac{\langle \varepsilon(x, y)\varepsilon^*(x + \Delta x, y + \Delta y)\rangle}{\langle I\rangle}, \tag{19}$$

$$g^{(2)}(\Delta x, \Delta y) = \frac{\langle I(x, y)I(x + \Delta x, y + \Delta y)\rangle}{\langle I\rangle^2}, \tag{20}$$

where the average intensity $\langle I\rangle$ is

$$\langle I\rangle = |B|^2\langle\sigma\rangle\int_{-\infty}^{\infty}\int_{-\infty}^{\infty} \mathrm{d}x_1\,\mathrm{d}y_1\,|h(x_1, y_1)|^2. \tag{21}$$

We are interested in the spatial correlation characteristics of the image, namely, $g^{(1)}(\Delta x, \Delta y)$ and $g^{(2)}(\Delta x, \Delta y)$.

The model in (10)–(21) implies that the spatial correlation of the 2D image is mainly determined by the spatial fluctuation of the number of scatterers N in a single resolution cell, the fluctuations of the scattered field $a_{x,y,i}$, and the impulse response function $h(x, y)$ of the imaging system in Figure 3. The spatial correlation coefficients $\rho^{(1)}(\Delta x, \Delta y)$ and $\rho^{(2)}(\Delta x, \Delta y)$ of RCS $\sigma(x, y)$ are determined by the spatial fluctuation of N and the disturbance of $a_{x,y,i}$. The next section summarizes the impact of these three factors on the spatial correlation of SAR images.

FLUCTUATION OF THE NUMBER OF SCATTERERS

This section explores the effect of the fluctuation of the number of scatterers on the correlation of the scattered field. According to the birth–death-migration model, the number of scatterers N can be described by a random variable with a negative binomial distribution. It was pointed out in [1] that, if the expectation of the negative binomial distribution was assumed to be an infinite constant, the K-distributed scattered field was obtained [4]; if the effect of the scattered phase was ignored, the coherent scatterer model would degenerate into a simpler incoherent scatterer sum model. The article approximated the scattered field as a noncoherent summation of multiple point scatterers. Under the assumption that N obeyed the negative binomial distribution with an infinite constant, the scattered field would obey a gamma distribution. This section first derives the distribution of the number of scatterers based on the birth–death-migration model, which is a negative binomial, and then introduces the influence of the number of scatterers on the spatial correlation property of the K- and gamma-distributed scattered fields.

DERIVATION OF NEGATIVE BINOMIAL DISTRIBUTION BASED ON THE BIRTH–DEATH-MIGRATION PROBLEM [4], [33]

The birth–death-migration problem can be described by the following rate equation [4], [33]:

$$\frac{dP_N}{\mathrm{d}t} = \mu(N + 1)P_{N+1} - [(\lambda + \mu)N + \nu]P_N + [\lambda(N - 1) + \nu]P_{N-1}, \tag{22}$$

where $P_N(t)$ denotes the probability that the number of scatterers is N at time t, λ is the birth rate, μ is the death rate, and ν is the immigration rate. The generating function of $P_N(t)$ is [4], [33]

$$Q(z, t) = \langle(1 - z)^N\rangle = \sum_{N=0}^{\infty}(1 - z)^N P_N(t). \tag{23}$$

Then, the partial differential equation of the generating function $Q(z, t)$ is

$$\frac{\partial Q}{\partial t} = z[-\mu + \lambda(1 - z)]\frac{\partial Q}{\partial z} - \nu z Q. \tag{24}$$

Assume that the number of scatterers at the initial time ($t = 0$) is M; that is, $P_N(0) = \delta(N - M)$. Replacing this condition in (23) obtains

$$Q(z; 0) = (1 - z)^M. \tag{25}$$

Since the sum of the probabilities is one, the second boundary condition can be written as

$$Q(0; t) = 1. \tag{26}$$

According to the two preceding boundary conditions, the instantaneous solution of the partial differential equation (24) is

$$Q(z, t) = \left(\frac{\lambda - \mu}{\lambda - \mu + \lambda(\theta - 1)z}\right)^{\frac{\nu}{\lambda}}\left(\frac{\lambda - \mu + (\mu\theta - \lambda)z}{\lambda - \mu + \lambda(\theta - 1)z}\right)^M, \tag{27}$$

where

$$\theta(t) = \exp[(\lambda - \mu)t]. \tag{28}$$

If $\mu > \lambda$ and $t \to \infty$, $\theta(\infty) = 0$, the equilibrium distribution is obtained:

$$Q(z, \infty) = (1 + \bar{N}z/\alpha)^{-\alpha}, \tag{29}$$

where $\bar{N} = \nu/(\mu - \lambda)$ and $\alpha = \nu/\lambda$. Then, according to $Q(z, \infty)$, the number of scatterers N obeys the negative binomial distribution:

$$p(N; \bar{N}, \alpha) = \binom{N + \alpha - 1}{N}\frac{\left(\frac{\bar{N}}{\alpha}\right)^N}{\left(1 + \frac{\bar{N}}{\alpha}\right)^{N+\alpha}}. \tag{30}$$

The author of [4] derived the correlation coefficient of the number of scatterers based on the joint generation function as

$$\frac{\langle N(0)N(t)\rangle-\bar{N}^2}{\bar{N}^2}=\left(\frac{1}{\alpha}+\frac{1}{\bar{N}}\right)\theta(t). \tag{31}$$

EFFECT OF THE NUMBER OF SCATTERERS THAT OBEY THE NEGATIVE BINOMIAL DISTRIBUTION ON THE CORRELATION FUNCTION OF THE SCATTERED FIELD [4], [33]

For the birth–death-migration model, assume that the number of random walks at the initial time t is N and that the number of random walks at time t' is N'. During the process from t to time t', a total of N_s steps survived, with an amplitude of $\{a_s\}$ and a phase of $\{\phi_s\}$; $(N-N_s)$ steps disappeared, with an amplitude of $\{a_d\}$ and a phase of $\{\phi_d\}$; and $(N'-N_s)$ steps were new, with an amplitude of $\{a_n\}$ and a phase of $\{\phi_n\}$. The correlation function of the complex scattered field can be written as [4], [33]

$$\begin{aligned}\left\langle E(t)E^*(t')\right\rangle=\Bigg\langle\Bigg(\sum_{N_s}a_s(t)e^{i\phi_s(t)}+\sum_{N-N_s}a_d(t)e^{i\phi_d(t)}\Bigg)\\ \times\Bigg(\sum_{N_s}a_s(t')e^{-i\phi_s(t')}+\sum_{N'-N_s}a_n(t')e^{-i\phi_n(t')}\Bigg)\Bigg\rangle.\end{aligned} \tag{32}$$

Assume that $\{\phi_s\}$, $\{\phi_d\}$, and $\{\phi_n\}$ are collectively independent, identically distributed random variables with a uniform distribution. Equation (32) can be simplified as

$$\begin{aligned}\left\langle E(t)E^*(t')\right\rangle=\langle N_s\rangle\left\langle a(t)a(t')\right\rangle\left\langle\exp i\left[\phi(t)-\phi(t')\right]\right\rangle,\\ t'=t+\tau,\quad \tau>0.\end{aligned} \tag{33}$$

If the initial number of scatterers decays with death rate μ, then the normalized first-order correlation function of the complex scattered field is

$$\rho^{(1)}(\tau)=\frac{\exp(-\mu\tau)\langle a(0)a(\tau)\rangle\langle\exp i[\phi(0)-\phi(\tau)]\rangle}{\langle a^2\rangle}, \tag{34}$$

where $\langle a(0)a(\tau)\rangle$ represents the spatial correlation of the amplitude a of a single scatterer and $\langle\exp i[\phi(0)-\phi(\tau)]\rangle$ characterizes the spatial correlation of the phase of a single scatterer. The normalized form of RCS correlation function $\left\langle\sigma(t)\sigma^*(t')\right\rangle$ is [4]

$$\begin{aligned}\rho^{(2)}(\tau)=1+\left(1+\frac{1}{\alpha}\right)|\rho^{(1)}(\tau)|^2+\left(\frac{1}{\alpha}+\frac{1}{\bar{N}}\right)\theta(\tau)\\ +\frac{1}{\bar{N}}\left(\frac{\langle a^2(0)a^2(\tau)\rangle}{\langle a^2\rangle^2}-1\right)\exp(-\mu\tau),\end{aligned} \tag{35}$$

where $\theta(t)$ is defined in (28).

The correlation functions $\rho^{(1)}(\tau)$ and $\rho^{(2)}(\tau)$ in the preceding are the results obtained based on the hypothesis of the negative binomial distribution, and these expressions characterize the relationship among the correlation function of scattered field, the number N of the scatterers that obey the negative binomial distribution, and the spatial correlation of a single scatterer. The correlation functions $\rho^{(1)}(\tau)$ and $\rho^{(2)}(\tau)$ can be extended to 2D cases, which are $\rho^{(1)}(\Delta x,\Delta y)$ and $\rho^{(2)}(\Delta x,\Delta y)$. The correlation information of the observed image $g^{(1)}(\Delta x,\Delta y)$ and $g^{(2)}(\Delta x,\Delta y)$ can be obtained by combining with the correlation effect introduced by the imaging impulse response, as presented in the next section.

THE CORRELATION FUNCTION OF THE K DISTRIBUTION

The K-distributed scattered field can be generated when the expectation of the negative binomial distribution satisfies $\bar{N}\to\infty$. Thus, the correlation function of K-distributed noise is obtained by letting $\bar{N}\to\infty$ in the correlation functions $\rho^{(1)}(\tau)$ and $\rho^{(2)}(\tau)$. Notice that $\rho^{(1)}(\tau)$ remains the same as in (34) and $\rho^{(2)}(\tau)$ can be further simplified as [4]

$$\rho^{(2)}(\tau)=1+\left(1+\frac{1}{\alpha}\right)|\rho^{(1)}(\tau)|^2+\frac{1}{\alpha}\theta(\tau), \tag{36}$$

where $\rho^{(2)}(\tau)$ consists of two parts: the perturbation term $\theta(\tau)$ of the number of scatterers and the interference term proportional to $|\rho^{(1)}(\tau)|^2$.

THE CORRELATION FUNCTION OF THE GAMMA DISTRIBUTION

If the influence of the phase of a single scatterer is ignored, the coherent scatterer model will degrade to the incoherent scatterer sum model [1], and RCS σ is modeled as a noncoherent sum of multiple point scatterers:

$$\sigma=\sum_{i=1}^{N}|a_i|^2. \tag{37}$$

There is no spatial correlation of complex scattered fields in the incoherent scatterer sum model; that is,

$$\rho^{(1)}(\tau)=0. \tag{38}$$

If it is assumed that the number of scatterers obeys the negative binomial distribution and its expectation value $\bar{N}\to\infty$, the RCS obeys a gamma distribution. The joint PDF $p(\sigma,\sigma')$ of the gamma distribution is

$$\begin{aligned}p(\sigma,\sigma')=\frac{\alpha^2}{\langle\sigma^2\rangle\Gamma(\alpha)(1-\theta)}\left(\frac{\alpha}{\langle\sigma\rangle}\sqrt{\frac{\sigma\sigma'}{\theta}}\right)^{-1}\\ \times\exp\left(-\frac{\alpha(\sigma+\sigma')}{\langle\sigma\rangle(1-\theta)}\right)I_{\alpha-1}\left(\frac{2\alpha\sqrt{\sigma\sigma'\theta}}{\langle\sigma\rangle(1-\theta)}\right),\end{aligned} \tag{39}$$

where $I_{\alpha-1}$ is the first modified Bessel function of order $\alpha-1$. According to the PDF in (39), the normalized correlation function of the RCS can be derived as [4]

$$\rho^{(2)}(\tau)=1+\frac{\theta(\tau)}{\alpha}. \tag{40}$$

It can be seen that the correlation function in (40) can also be obtained by the K-distributed correlation function $\rho^{(2)}(\tau)$ in (36) by ignoring the term with $|\rho^{(1)}(\tau)|^2$.

FLUCTUATION OF A SINGLE SCATTERER

This section explores the correlation modeling of the scattered field $a_{x,y,i}$ of a single scatterer and its influence on the correlation characteristics of RCS σ. There are currently two methods for modeling $a_{x,y,i}$: physical and

statistical. The author of [7] proposed four physical models for $a_{x,y,i}$, while [32] modeled $a_{x,y,i}$ from a statistical perspective by assuming that it followed a correlated gamma law. Both approaches provide analytical expressions of the correlation function of the RCS, which are expressed in 1D form.

PHYSICAL MODELING OF A SINGLE SCATTERER

The four physical models for the scattered field $a_{x,y,i}$ of a single scatterer in [7] are as follows:

- narrowband thermal noise with a single coherence length ℓ_c
- the mixture of two narrowband noise processes that have the same center frequency but different correlation lengths, ℓ_a and ℓ_b, and cross sections σ_a and σ_b
- narrowband thermal noise of intensity σ_s and a single coherence length ℓ_c, mixed with a local oscillator of strength σ_0 shifted by a frequency ω
- the mixture of two narrowband noise sources with the same correlation length ℓ_c and the same cross section but with their center frequencies offset by ω.

In [7], the author provided the correlation function $\rho^{(2)}(\Delta x, \Delta y)$ of the RCS based on the four preceding physical models. The author also presented the correlation function $g^{(2)}(\Delta x, \Delta y)$ of the observed image through a rectangular imaging impulse function.

STATISTICAL MODELING OF A SINGLE SCATTERER

The statistical modeling of a single scatterer assumes that the scattered field of each scatterer obeys a correlated gamma distribution and the correlation information of the RCS can be derived using an incoherent scatterer sum model [32]. For convenience, rewrite the incoherent scatterer sum model in (37) as

$$\sigma = \sum_{i=1}^{N} z_i = \sum_{i=1}^{N} |a_i|^2, \tag{41}$$

where z_i is the scattered field of the ith scatterer in a resolution cell. It is assumed that z_i obeys a gamma distribution with a mean of μ_z, a variance of s_z^2, and a correlation coefficient of ρ_z. Here, N is a random variable that obeys a negative binomial distribution with a mean of μ_N and a variance of s_N^2, which is independent from z_i. The preceding equation can be regarded as a local sum process (LSP) in a window with N scatterers.

The sum of independent gamma variables still obeys a gamma distribution; however, the sum of correlated gamma variables is no longer granted this property. The probability distribution after summing is usually difficult to obtain [34], [35]. The authors of [32] used the approximation that the sum of the correlated gamma variables is still gamma distributed and derived the correlation function of the RCS σ as [32], [36]

$$\langle \sigma(t)\sigma(t-r)\rangle = \langle N^2\rangle \mu_z^2 + s_z^2 \left\langle \sum_{i=1}^{N(t)} \sum_{j=1}^{N(t-r)} \rho_z(i,j,r) \right\rangle, \tag{42}$$

where r is the spatial distance between two pixels, $\langle N^2\rangle$ is the second-order moment of N, and $\rho_z(i,j,r)$ is the correlation coefficient between the ith scatterer in one resolution cell and the jth scatterer in another resolution cell at distance r.

The corresponding correlation coefficient of the RCS is [32], [36]

$$\begin{aligned}
&\rho_\sigma(r) = \gamma(N,r)\left(\frac{\mu_z^2}{\sigma_z^2 \mu_N} + \gamma(N)\right)^{-1}, r \geq w, \text{in which} \\
&\gamma(N) = \frac{1}{\mu_N} + \frac{1}{\mu_N^2}\left\langle \sum_{i=1}^{N}\sum_{\substack{j=1 \\ j\neq i}}^{N} \rho_z(i,j,r=0) \right\rangle, \text{and} \\
&\gamma(N,r) = \frac{1}{\mu_N^2}\left\langle \sum_{i=1}^{N(t)}\sum_{j=1}^{N(t-r)} \rho_z(i,j,r) \right\rangle, r \geq w,
\end{aligned} \tag{43}$$

where w is the window size of the LSP, and it is valid when $r \geq w$. Notice that $\gamma(N,r)$ is the variance function and $\rho_z(i,j,r=0)$ is the correlation coefficient between the ith and the jth scatterer in a resolution cell.

Passing the RCS σ that obeys a gamma distribution through the imaging impulse response $h(x)$, the correlation function of the observed image intensity is [2], [32]

$$\begin{aligned}
\langle I(x)I(x+X)\rangle = \langle\sigma\rangle^2 \times \Bigg\{ & 1 + \left| \int_{-\infty}^{\infty} h(x-\xi)h^*(x+X-\xi)\mathrm{d}\xi \right|^2 \\
& + \int_{-\infty}^{\infty}\int_{-\infty}^{\infty} \frac{\rho_\sigma(\xi_2-\xi_1)}{\nu} |h(x-\xi_1)|^2 \\
& \times |h(x+X-\xi_2)|^2 \mathrm{d}\xi_1 \mathrm{d}\xi_2 \\
& + \int_{-\infty}^{\infty}\int_{-\infty}^{\infty} \frac{\rho_\sigma(\xi_2-\xi_1)}{\nu} h(x-\xi_1)h^*(x+X-\xi_1) \\
& \times h^*(x-\xi_2)h(x+X-\xi_2)\mathrm{d}\xi_1\mathrm{d}\xi_2 \Bigg\},
\end{aligned} \tag{44}$$

where σ obeys a gamma distribution with order parameter ν and ρ_σ is the autocorrelation function of σ in (43). The first two terms of (44) describe the results of the coherent imaging of constant background and independent point scatterers; the third term defines the effect of the imaging process on the RCS, and the fourth term defines the coherent imaging. What needs to be determined in (44) are the autocorrelation function ρ_σ of σ and the impulse response function $h(x)$ of the imaging system.

IMAGING IMPULSE RESPONSE

The expression of the correlation coefficient of the 2D complex image ε is [9]

$$\begin{aligned}
g^{(1)}(\Delta x, \Delta y) = & \int_{-\infty}^{\infty}\int_{-\infty}^{\infty}\int_{-\infty}^{\infty}\int_{-\infty}^{\infty} dx_1\,dx_2\,dy_1\,dy_2 \\
& \times \langle A(x_1,y_1)A^*(x_2,y_2)\rangle \langle e^{j[\theta(x_1,y_1)-\theta(x_2,y_2)]}\rangle \\
& \times h(x_1,y_1)h^*(x_2,y_2) \\
& \left(\langle\sigma\rangle \int_{-\infty}^{\infty}\int_{-\infty}^{\infty} dx_1\,dy_1 |h(x_1,y_1)|^2\right)^{-1},
\end{aligned} \tag{45}$$

where $\langle A(x_1,y_1)A^*(x_2,y_2)\rangle = \langle\sigma\rangle$. Assuming that the scatterers in a single resolution cell are randomly distributed and ignoring the effect of the phase, the preceding formula can be simplified as [9]

$$g^{(1)}(\Delta x,\Delta y)=\frac{\int_{-\infty}^{\infty}\int_{-\infty}^{\infty}\mathrm{d}x_1\,\mathrm{d}y_1 h(x_1,y_1)h^*(x_1+\Delta x,y_1+\Delta y)}{\int_{-\infty}^{\infty}\int_{-\infty}^{\infty}\mathrm{d}x_1\,\mathrm{d}y_1|h(x_1,y_1)|^2}. \tag{46}$$

It can be seen that the correlation function $g^{(1)}(\Delta x,\Delta y)$ is independent of the RCS and that it is only a function of the imaging impulse response.

The correlation coefficient of the intensity image I is [9]

$$\begin{aligned}g^{(2)}(\Delta x,\Delta y)=1+&\left|g^{(1)}(\Delta x,\Delta y)\right|^2\\&+\int_{-\infty}^{\infty}\int_{-\infty}^{\infty}\int_{-\infty}^{\infty}\int_{-\infty}^{\infty}\mathrm{d}x_1\,\mathrm{d}x_2\,\mathrm{d}y_1\,\mathrm{d}y_2\\&\times\left(\frac{\langle\sigma(x_1,y_1)\sigma(x_2,y_2)\rangle}{\langle\sigma\rangle^2}-1\right)\\&\times\left(\int_{-\infty}^{\infty}\int_{-\infty}^{\infty}dx_1dy_1|h(x_1,y_1)|^2\right)^{-2}\\&\times\left[|h(x_1,y_1)|^2|h(x_2+\Delta x,y_2+\Delta y)|^2\right.\\&+h(x_1,y_1)h^*(x_1+\Delta x,y_1+Y)\\&\left.h(x_2,y_2)h^*(x_2+\Delta x,y_2+\Delta Y)\right].\end{aligned} \tag{47}$$

The first term of (47) describes the correlation caused by the constant intensity due to coherent speckle noise, which is independent of the RCS. The second term is also independent of the RCS and is determined by the imaging impulse response function. The third and fourth terms combine the influence of both the RCS and the imaging impulse response. The second and third terms decay rapidly under the influence of the imaging impulse response function. The fourth term can be regarded as the convolution of the variation of RCS and the imaging impulse response [12]. Equation (47) shows that the correlation of the observed image intensity is determined by the correlation of the RCS and the imaging impulse response function. If the spatial variation of the RCS is ignored, the RCS retains only the first two terms, which can be simplified as

$$g^{(2)}(\Delta x,\Delta y)=1+\left|g^{(1)}(\Delta x,\Delta y)\right|^2. \tag{48}$$

The most common 2D imaging impulse response functions $h(x,y)$ are the sinc, the Gaussian, and the rectangular functions introduced in the following:

1) The 2D sinc point spread function (PSF) $h_{\mathrm{sinc}}(x,y)$ can be separated into slant range PSF $h_r(y)$ and azimuth PSF $h_a(x)$ as [2]

$$h_{\mathrm{sinc}}(x,y)=h_a(x)h_r(y), \tag{49}$$

where

$$\begin{aligned}h_r(t)&=(\tau_p-|t|)\ \mathrm{sinc}\left(\frac{\beta}{\pi}t[\tau_p-|t|]\right)\mathrm{rect}\left(\frac{t}{\tau_p}\right)\\&\cong\tau_p\,\mathrm{sinc}(Bt)\end{aligned} \tag{50}$$

and

$$h_a(x)=\exp(i\beta x^2)\int_{-\infty}^{\infty}a\left(-\frac{y}{R_0}\right)W\left(\frac{x-y}{R_0}\right)\exp(-2i\beta xy)\,\mathrm{d}y, \tag{51}$$

where τ_p is the pulse length, β is the focusing parameter, B is the bandwidth, R_0 is the slant range, $a(\phi)$ is the two-way amplitude azimuth antenna pattern, $W(\phi)=\mathrm{rect}(\phi/\psi_a)$, and ψ_a is the azimuth beamwidth.

2) The 2D Gaussian PSF $h_G(x,y)$ can be expressed as [8]

$$|h_G(x,y)|=\exp\left[-\frac{x^2}{w_x^2}-\frac{y^2}{w_y^2}\right], \tag{52}$$

where w_x and w_y are the azimuth and range widths, respectively.

3) The rectangular PSF $h_{\mathrm{rect}}(x,y)$ is

$$h_{\mathrm{rect}}(x,y)=\begin{cases}1, & -\frac{\ell}{2}<y<\frac{\ell}{2}\\0, & \text{else.}\end{cases} \tag{53}$$

CORRELATED SAR CLUTTER SIMULATION

This section introduces the main methods of correlated clutter simulation based on single-pixel and correlated statistical modeling. SAR image simulation is a forward process for modeling the imaging procedure, and it is an important method for analyzing the validity and accuracy of the proposed statistical modeling [21]–[27]. Combining the two spatial correlation models introduced in the previous section, this section describes the corresponding correlated clutter simulation methods, namely, the correlated clutter simulation method based on the product model [37] and the correlated clutter simulation method based on the coherent scatterer model [32]. We also put in perspective the correlated clutter simulation method recently proposed by Yue et al. [38] based on a GGCS. This approach provides a more general modeling technique for correlated clutter. In addition, the correlated clutter simulation method based on the ITM [30] is an approach that can be used to simulate arbitrary probability distributions and correlation structures. Its theory and main steps are introduced in this section.

The correlated clutter simulation methods introduced in this section are mainly based on two widely used distributions: K and G^0 [2], [13], [31]. The K distribution is often used to describe data that have strong contrast, such as forests and sea surfaces, but it can seldom be used to detail areas with extremely strong contrast, including urban locations [2], [13]. The G^0 distribution can be employed to describe extremely strong contrast and inhomogeneous regions, such as urban areas, primary forests, and deforested locations [31]. Both the K and G^0 distributions are based on the product model, which is a common framework adopted in coherent illumination. Sampling from these distributions is straightforward using the product model, as the distributions are the product and the quotient, respectively, of two independent gamma deviates. This leads to the ability to build fields that obey independent K and G^0 distributions. In particular, the G^0 distribution admits several sampling strategies [39].

A common feature in SAR data is the lack of independence among neighboring observations. This spatial correlation is one of the ways the elusive notion of texture manifests [9]. Since simulating plausible outcomes from a variety of targets

is usually necessary, it is mandatory to develop techniques for sampling correlated K and G^0 fields. The easiest way of introducing correlation in a field of independent deviates is to apply a convolution mask. This approach is not feasible for our problem because neither the K nor the G^0 distributions are preserved by the convolution operation. Therefore, indirect methods are necessary for introducing correlation between K and G^0 deviates, which is the topic of this section.

SIMULATION BASED ON THE PRODUCT MODEL

This section introduces correlated clutter simulation methods based on the product model. Such observations can be easily obtained by separately simulating the correlated RCS component and the speckle component and then multiplying them. There is a variety of distributions to model the RCS [1], and the most widely used is the gamma law. The N-look speckle is generally modeled as a gamma distribution with a unitary mean and the shape parameter N. An RCS that obeys the correlated gamma distribution multiplied by the uncorrelated gamma-distributed speckle generates correlated K-distributed SAR clutter. These components comprise the two steps of the main methods for sampling from correlated K clutter. Figure 4 conveys a correlated clutter simulation flowchart based on the product model discussed in this section. The generation of correlated gamma-distributed samples is a basic problem in SAR image simulation. The authors of [2] summarize four methods for generating correlated gamma deviates: filtering uncorrelated gamma-distributed noise [40], applying the random walk model [7], resampling from correlated exponential-distributed variables [41], and resampling from correlated Gaussian-distributed variables [2], [42].

FILTERING UNCORRELATED GAMMA-DISTRIBUTED NOISE

The method based on filtering uncorrelated gamma-distributed noise [40] obtains the correlated gamma samples by convolving uncorrelated gamma deviates using a specific filter. Passing independent, identically distributed random variables through a moving-average filter of size L produces correlated random variables with a triangular autocorrelation function. However, arbitrary filters do not grant the preservation of the original distribution. To preserve the statistical characteristics of the gamma distribution, the convolution filter has to have equal weights, that is, a simple moving-average filter. This restricts the ability to produce complex correlated structures. Also, it is difficult to determine the filter to be applied. The main idea of filtering uncorrelated gamma-distributed noise is described in the following by taking two identically distributed gamma random variables with mean μ, order ν, and correlation coefficient ρ, as in [40].

The moment-generating function of gamma distribution can be written as [43]

$$\Phi(s) = \left(1 - \frac{\mu}{\nu} s\right)^{-\nu}. \tag{54}$$

The moment-generating function of two gamma distributions with correlation coefficient ρ is [40]

$$\begin{aligned}\Phi(s_1, s_2) &= \left(1 - \frac{\mu}{\nu} s_1\right)^{-\nu(1-\rho)} \left(1 - \frac{\mu}{\nu} s_2\right)^{-\nu(1-\rho)} \times \left(1 - \frac{\mu}{\nu}(s_1 + s_2)\right)^{-\nu\rho} \\ &= \left(1 - \frac{\mu(1-\rho)}{\nu(1-\rho)} s_1\right)^{-\nu(1-\rho)} \left(1 - \frac{\mu(1-\rho)}{\nu(1-\rho)} s_2\right)^{-\nu(1-\rho)} \\ &\quad \times \left(1 - \frac{\mu\rho}{\nu\rho}(s_1 + s_2)\right)^{-\nu\rho}. \end{aligned} \tag{55}$$

The first two terms of the moment-generating function of the preceding formula can be regarded as the joint moments of two identically distributed gamma random variables with mean $\mu(1-\rho)$ and order $\nu(1-\rho)$. The third term is the joint moment of two independent gamma random variables with mean $\mu\rho$ and order $\nu\rho$. The

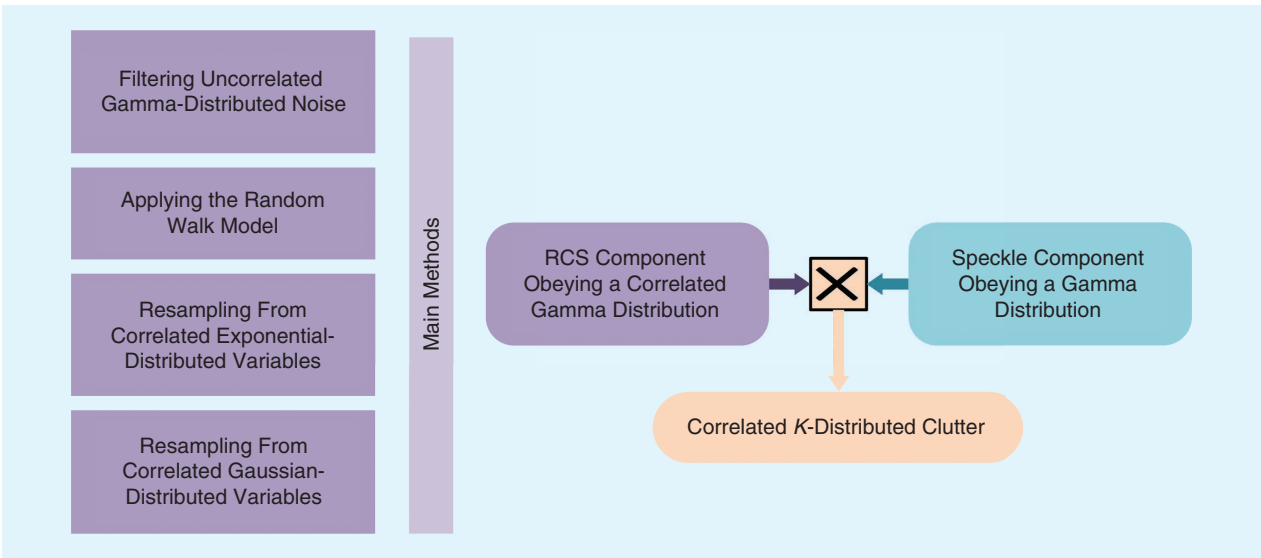

FIGURE 4. A correlated K-distributed clutter simulation based on the product model.

product of the joint moments represents the sum of the random variables. Therefore, the steps for sampling two identically distributed gamma random variables with mean μ, order v, and correlation coefficient ρ are [40] as follows:

1) sampling from X_1, which follows a gamma distribution with mean $\mu(1-\rho)$ and order $v(1-\rho)$
2) sampling from X_2, which follows a gamma distribution with mean $\mu(1-\rho)$ and order $v(1-\rho)$
3) sampling from Y, which follows a gamma distribution with mean $\mu\rho$ and order $v\rho$
4) samples that obey the desired bivariate gamma distribution with correlation ρ are (X_1+Y, X_2+Y).

APPLYING THE RANDOM WALK MODEL

This method [7] generates correlated gamma deviates by summing squared correlated Gaussian random variables. It is based on the fact that the sum of n squared standard Gaussian random variables $\xi_j \sim \mathcal{N}(0, 1/2)$ with same correlation coefficient $\rho/2$,

$$\eta_i = \sum_{j=1}^{n} \xi_j^2, \tag{56}$$

obeys a gamma distribution with shape parameter $n/2$ and correlation ρ^2, denoted as $\eta_i \sim \Gamma(n/2, 1)$ [43]. Then, $X = \beta_i^{-1}\eta_i$ obeys a correlated gamma distribution with marginal probability distribution $\Gamma(n/2, \beta_i)$ and correlation coefficient $\rho_{i,j}^2$. The disadvantage of this method is that it is applicable only to the case where the order parameter is a semi-integer, and thus it cannot simulate arbitrary textures.

RESAMPLING FROM CORRELATED EXPONENTIAL-DISTRIBUTED VARIABLES

Denoting G and γ as a Gaussian-distributed variable and an exponential-distributed variable, respectively, this method first obtains exponential deviates with correlation coefficient $\rho_\gamma = |\rho_G|^2$ from the sum of the squares of two Gaussian observations with correlation coefficient ρ_G and then resamples the gamma-distributed variable σ with correlation coefficient ρ_σ by the inverting the following expression [2], [41]:

$$\gamma(\nu, \sigma) = \Gamma(\nu)\left(1 - \exp\left[-\frac{\nu\gamma}{\mu}\right]\right), \tag{57}$$

where $\Gamma(\cdot)$ is gamma function and μ and ν are the mean and the order of the gamma distribution, respectively. Here, $\gamma(\cdot)$ is an incomplete gamma function [44]:

$$\gamma(\nu, \sigma) = \int_0^\sigma e^{-t} t^{\nu-1} dt. \tag{58}$$

The relationship between the correlation coefficient ρ_σ of the gamma-distributed variable and the correlation coefficient ρ_γ of the negative exponential input is as follows [2], [41]:

$$\rho_\sigma = \frac{\langle \sigma_1 \sigma_2 \rangle - \langle \sigma \rangle^2}{\langle \sigma^2 \rangle - \langle \sigma \rangle^2} = \begin{cases} 0; \ \rho_\gamma = 0 \\ \nu\{(1-\rho_\gamma)^{\nu+2} \, {}_2\mathrm{F}_1(\nu+1, \nu+1; \nu; \rho_\gamma) - 1\}; 0 < \rho_\gamma < 1, \\ 1; \ \rho_\gamma = 1 \end{cases} \tag{59}$$

where ${}_2\mathrm{F}_1[\cdot]$ is the hypergeometric function [2], [45]. It should be noted that a typo in [2, eq. (5.27)] is corrected in (59). The disadvantage of this resampling method is that it is difficult to invert (59). Since the square root of any correlation function is not necessarily valid itself, it is not suitable for arbitrary correlation functions.

RESAMPLING FROM CORRELATED GAUSSIAN-DISTRIBUTED VARIABLES

The three methods described previously can be used only for positive correlation coefficients, not for negative correlation characteristics, such as shaded areas. The Gaussian resampling method can generate negative correlation structures [2], [42], [46]. This approach [2] first generates an uncorrelated Gaussian random sample image, then convolves a specific convolution kernel to obtain the correlated Gaussian sample γ. Finally, it applies a composition of functions: the cumulative distribution function (CDF) of the Gaussian distribution (which produces uniform deviates) and the inverse of the CDF of the desired marginal gamma distribution function, thus obtaining the desired correlated gamma field. The desired correlation structure stipulates the convolution kernel through a relationship that involves inverting integral equations. After generating the correlated RCS component of the gamma distribution, uncorrelated gamma-distributed speckle with a unitary mean and a shape parameter n is straightforward to simulate. And it is then multiplied with the correlated RCS components to obtain a correlated clutter image based on the product model.

SIMULATION BASED ON THE ITM

Differing from the approach of separately simulating the RCS and the speckle components in the product model, simulation based on the ITM directly generates correlated clutter based on the known single-pixel probability distribution and the correlation coefficient. The simplest part is sampling from the single-pixel distribution. The difficulty lies in how to stipulate the desired correlation structure. The easiest way to introduce correlation is to pass independent random deviates through a convolution operation. However, since K and G^0 distributions are not convolution invariant, this method cannot be used. In this case, it is necessary to rely on an indirect method, the ITM, to introduce correlation. The advantage of the ITM is that it can generate random fields of arbitrary correlation structure. Bustos et al. [30] proposed a correlated G_A^0 (the subscript $_A$ denotes amplitude) distributed clutter simulation approach based on the ITM.

Since the easiest way to control correlation is by using Gaussian random variables, the main point of the ITM can be summarized in two steps: first, produce correlated Gaussian observations by building a convolution mask that is applied to a field of independent, identically distributed, zero-mean Gaussian variables with unitary variance, then transform these correlated Gaussian variables into a field of correlated K or G_A^0 samples by inversion. The core of this indirect method is how to calculate the correlation of the Gaussian random field according to the desired final correlation. This section introduces the mathematical model of the ITM, followed by the main steps of simulating correlated G^0-distributed clutter based on the ITM.

ITM THEORY

The ITM mainly uses the following two theorems. The first [43] provides a method for obtaining a uniformly distributed random variable from an arbitrarily distributed continuous random variable. The second is a way of transforming a uniformly distributed random variable in $(0,1)$ into an arbitrarily distributed random variable.

THEOREM 1: ARBITRARY CONTINUOUS DISTRIBUITON TO UNIFORM DISTRIBUTION

As shown in Figure 5(a), let V be any continuous random variable, with CDF $F_V(v) = P\{V \le v\}$. Define the random variable $U = F_V(v)$. Then, U follows a uniform distribution in (0,1).

THEOREM 2: UNIFORM TO ARBITRARY DISTRIBUTION

In Figure 5(a), denote A as a random variable with CDF $F_A(a) = P\{A \le a\}$. The inverse function of the CDF is expressed as F_A^{-1}. Designate U as a random variable that obeys a uniform distribution, namely, $U \sim \mathcal{U}(0,1)$. If $W = F_A^{-1}(U)$, W obeys the distribution characterized by F_A.

The relationship of the random variables in the preceding theorems, which is described in Figure 5(a), leads to the ITM. It gives an indirect method for sampling from the random variable W with CDF F_A based on an arbitrary variable V. For the clutter simulation problem, a random process $G_\sigma^0(\alpha,\gamma,n)$ is used to describe the intensity field Z_σ of the SAR image, which is labeled as $Z_\sigma \sim (G_\sigma^0(\alpha,\gamma,n), \rho_{Z_\sigma})$, where ρ_{Z_σ} is the correlation function of the G_σ^0-distributed random variables. Since it is not possible to generate G_σ^0-distributed correlated random variables by convolution, using the ITM described previously is a good choice. Since the Gaussian distribution is the simplest distribution invariant with respect to the convolution operation, V in Figure 5(a) is selected to be a Gaussian random variable denoted by ζ in Figure 5(b). As shown in Figure 5(b), denote the CDF of ζ as Φ; then, $U = \Phi(V)$ obeys the uniform distribution, according to Theorem 1. Denote the CDF of G_σ^0 as $F_{G_\sigma^0}$ and its inverse function as $F_{G_\sigma^0}^{-1}$; $F_{G_\sigma^0}^{-1}(U)$ obeys the G_σ^0 distribution, according to Theorem 2.

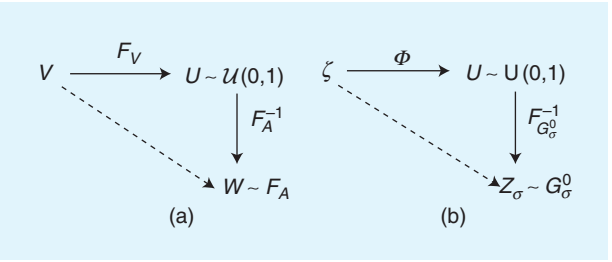

FIGURE 5. The relationship in the ITM. (a) ITM theory. (b) ITM theory based on Gaussian random variable.

The process of simulating an image of size $C \times C$ in which each sample $Z_\sigma(i,j)$ obeys the G_σ^0 distribution can be expressed as [30]

$$Z_\sigma(i,j) = F_{G_\sigma^0}^{-1}(\Phi(\zeta(i,j))), \tag{60}$$

where $\zeta = (\zeta(i,j))_{0 \le i \le C-1, 0 \le j \le C-1}$ is a stochastic process and $\zeta(i,j)$ is a standard Gaussian random variable with correlation function τ_ζ. The CDF $F_{G_\sigma^0}(\cdot,(\alpha,\gamma,n))$ and its inverse $F_{G_\sigma^0}^{-1}$ of $G_\sigma^0(\alpha,\gamma,n)$ are, respectively, expressed as [30]

$$F_{G_\sigma^0}(z,(\alpha,\gamma,n)) = \Upsilon_{2n,-2\alpha}\left(-\frac{\alpha z}{\gamma}\right), \tag{61}$$

$$F_{G_\sigma^0}^{-1}(t,(\alpha,\gamma,n)) = -\frac{\gamma}{\alpha}\Upsilon_{2n,-2\alpha}^{-1}(t), \tag{62}$$

where Υ_{v_1,v_2} is the CDF of a Fisher–Snedecor F_{v_1,v_2} distribution; i.e.,

$$\Upsilon_{v_1,v_2}(x) = \frac{\Gamma\left(\frac{v_1+v_2}{2}\right)}{\Gamma\left(\frac{v_1}{2}\right)\Gamma\left(\frac{v_2}{2}\right)}\left(\frac{v_1}{v_2}\right)^{\frac{v_1}{2}} \times \int_0^x t^{\frac{v_1-2}{2}}\left(1+\frac{v_1}{v_2}t\right)^{-\frac{v_1+v_2}{2}} dt. \tag{63}$$

Another important problem is the correspondence between the correlation coefficients ρ_{Z_σ} of Z_σ and τ_ζ of the Gaussian random variable ζ. Analogous to the derivation in [30], we obtain

$$\rho_{Z_\sigma}((i,j),(k,l)) = \varrho_{(\alpha,n)}(\tau_\zeta((i,j),(k,l))), \tag{64}$$

$$\varrho_{(\alpha,n)}(\tau) = \frac{R_{(\alpha,n)}(\tau) - \left(\frac{1}{-\alpha-1}\right)^2}{\frac{n+\alpha+1}{n(\alpha+1)^2(\alpha+2)}}, \tau \in (-1,1), \tag{65}$$

where

$$R_{(\alpha,n)}(\tau) = \iint F_{G_\sigma^0}^{-1}(\Phi(u),(\alpha,1,n))F_{G_\sigma^0}^{-1}(\Phi(v),(\alpha,1,n)) \times \phi_2(u,v,\tau)\mathrm{d}u\mathrm{d}v, \tag{66}$$

$$\phi_2(u,v,\tau) = \frac{1}{2\pi\sqrt{(1-\tau^2)}}\exp\left(-\frac{u^2-2\tau\cdot u\cdot v+v^2}{2(1-\tau^2)}\right). \tag{67}$$

CORRELATED G^0-DISTRIBUTED CLUTTER

The detailed steps for generating a random field with a correlated G_σ^0 distribution based on the ITM are documented in the following. As presented in Figure 6, the main idea [30], [31] is to first generate a correlated Gaussian random field, then convert it to the correlated G_σ^0 distribution using the ITM. The correlated Gaussian random field is produced using the Fourier transform (the Fourier transform of the correlation function is the square of the power spectral density).

1) Propose the desired correlation structure ρ_{Z_σ} for G_σ^0. Denote the simulated SAR image as

$$Z_\sigma = (Z_\sigma(k,\ell))_{0\le k\le N-1, 0\le \ell\le N-1},$$

which is controlled by a random process $\xi_\sigma^0(\alpha,\gamma,n)$ with correlation function ρ_{Z_σ}:

$$\rho_{Z_\sigma}((k_1,\ell_1),(k_2,\ell_2)) = \rho(k_2-k_1,\ell_2-\ell_1),$$
$$\text{for every } -(N-1)\le k_2-k_1,\ell_2-\ell_1\le N-1. \tag{68}$$

Given the sets

$$R_1 = \left\{(k,\ell): 0\le k,\ell\le \frac{N}{2}\right\},$$
$$R_2 = \left\{(k,\ell): \frac{N}{2}+1\le k\le N-1, 0\le \ell\le \frac{N}{2}\right\},$$
$$R_3 = \left\{(k,\ell): 0\le k\le \frac{N}{2}, \frac{N}{2}+1\le \ell\le N-1\right\},$$
$$R_4 = \left\{(k,\ell): \frac{N}{2}+1\le k\le N-1, \frac{N}{2}+1\le \ell\le N-1\right\},$$
$$R_N = R_1\bigcup R_2\bigcup R_3\bigcup R_4 = \{(k,l): 0\le k,\ell\le N-1\},$$
$$\overline{R_N} = \{(k,\ell): -(N-1)\le k,l\le N-1\}, \tag{69}$$

let $\rho: R_1\to(-1,1)$ be a function with domain R_1 and a range $(-1,1)$, which can be extended to $\overline{R_N}$ according to the following expression:

$$\rho(k,\ell) = \begin{cases} \rho(N-k,\ell) & \text{if } (k,\ell)\in R_2,\\ \rho(k,N-\ell) & \text{if } (k,\ell)\in R_3,\\ \rho(N-k,N-l) & \text{if } (k,\ell)\in R_4,\\ \rho(N+k,\ell) & \text{if } -(N-1)\le k<0\le \ell\le N-1,\\ \rho(k,N+\ell) & \text{if } -(N-1)\le \ell<0\le k\le N-1,\\ \rho(N+k,N+\ell) & \text{if } -(N-1)\le k,\ell<0. \end{cases} \tag{70}$$

2) Calculate the correlation structure $\tau_\zeta(k,\ell)$ for the Gaussian random field by inverting (64):

$$\tau_\zeta(k,\ell) = \eth_{(\alpha,n)}(\rho_{Z_\sigma}(k,\ell)). \tag{71}$$

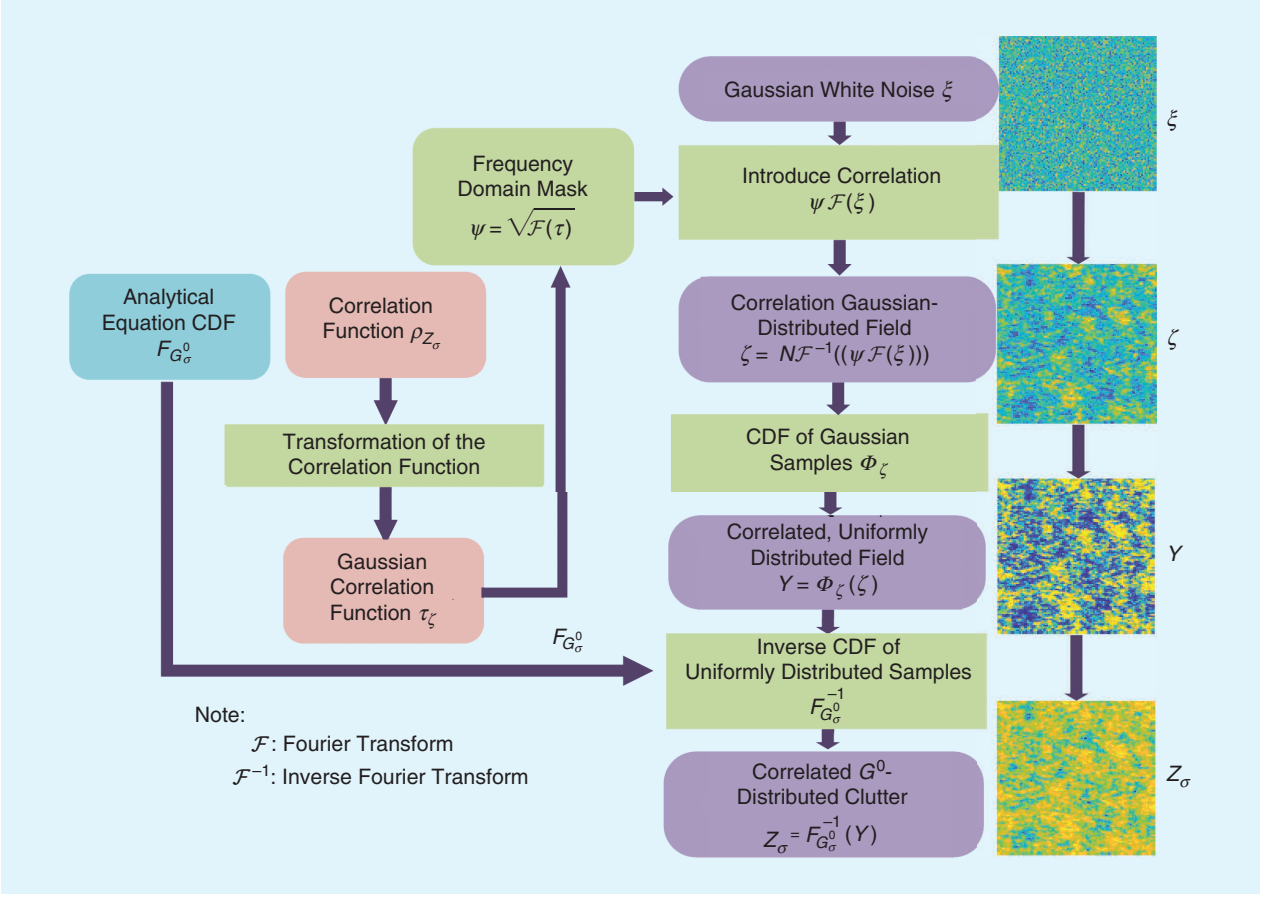

FIGURE 6. A correlated G_A^0 clutter simulation based on the ITM.

3) Calculate the mask $\psi(k,\ell)$ in the frequency domain of the correlation structure τ_ζ as

$$\psi(k,v) = \sqrt{\mathcal{F}(\tau_\zeta)(k,\ell)}, \tag{72}$$

where $\mathcal{F}(\tau_\zeta)$:$R_N \to \mathbb{C}$ is the normalized Fourier transform for τ_ζ:

$$\mathcal{F}(\tau_\zeta)(k,\ell) = \frac{1}{N^2}\sum_{k_1=0}^{N-1}\sum_{\ell_1=0}^{N-1}\tau_\zeta(k_1,\ell_1) \times \exp(-2\pi i(k\cdot k_1 + l\cdot \ell_1)/N^2). \tag{73}$$

4) Generate Gaussian white noise with zero mean and unit variance:

$$\xi = (\xi(k,\ell))_{(k,\ell)\in R_N}. \tag{74}$$

5) Generate a Gaussian random field with correlation structure τ_ζ. Take the Fourier transform of the Gaussian white noise ξ and introduce the correlation in the frequency domain using the mask $\psi(k,\ell)$, and, finally, obtain the correlated Gaussian random field by the inverse Fourier transform. The Gaussian stochastic process with correlation structure $\tau_\zeta(k,\ell)$ is

$$\zeta(k,\ell) = N\mathcal{F}^{-1}((\psi\mathcal{F}(\xi)))(k,\ell), \tag{75}$$

where $\mathcal{F}$ is Fourier transformation operator and $\mathcal{F}^{-1}$ is the inverse Fourier transformation operator.

6) Generate the $Z_\sigma^1(k,\ell)$ field with the correlation structure $\rho_{Z_\sigma}(k,\ell)$ that obeys the $G_\sigma^0(\alpha,1,n)$ distribution using the ITM, which is

$$Z_\sigma^1((k,\ell)) = F_{G_\sigma^0}^{-1}(\Phi(\zeta((k,\ell))),(\alpha,1,n)). \tag{76}$$

7) Generate the $Z_\sigma(k,\ell)$ field with the correlation structure $\rho_{Z_\sigma}(k,\ell)$ that obeys the $G_\sigma^0(\alpha,\gamma,n)$ distribution by $Z_\sigma(k,\ell) = \gamma Z_\sigma^1(k,\ell)$.

There are two shortcomings of the clutter simulation method based on the ITM proposed by Bustos et al. [30] in practical applications: 1) for new types of scenes, the relevant formula needs to be derived, and 2) there are many statistical distributions and textures in real scenes, and deriving the analytical expressions for every distribution may be too demanding. To solve this problem, [47] presented a semantic–statistical convolution scheme to generate an SAR image based on a semantic map, which avoids complex derivations and is suitable for areas with various kinds of terrain. The main goal of this method is to generate a new SAR clutter sample with the same single-pixel probability distribution and correlated structure as the given sample.

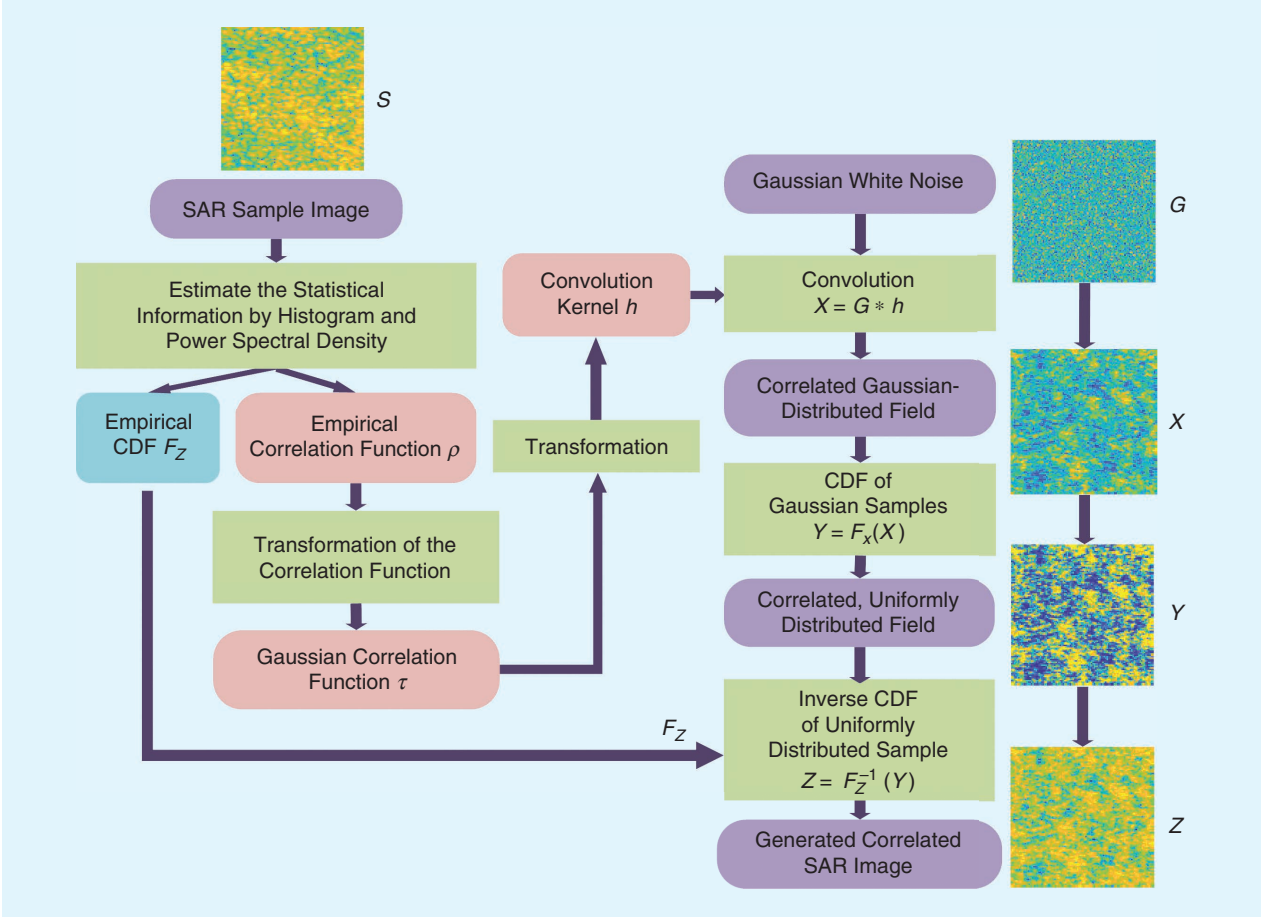

FIGURE 7. A correlated clutter simulation based on semantic–statistical convolution.

The entire process is realized through numerical simulation. The main steps are shown in Figure 7 and are as follows:

1) Estimate CDF F_Z and correlation structure ρ of the SAR image S. The CDF is estimated by the empirical CDF of the sample; correlation structure ρ is obtained from the inverse Fourier transform of the power spectral density of the sample [43]:

$$\rho = \mathcal{F}^{-1}(|\mathcal{F}(S)|^2). \tag{77}$$

2) Determine correlation structure τ to be imposed to the Gaussian field to observe the desired correlation structure ρ in the field Z. Experiments show that the relationship between τ and ρ lies in approximately linear areas with low to moderate contrast; in such cases, take as τ the same ρ. Areas with extreme contrast, such as urban locations, depart from this linear relationship; in those instances, look up the inversion tables in [30] and [37]. The correlation structure τ and the convolution kernel h satisfy the following relationship [43]:

$$\tau(k,\ell) = h(k,\ell) \circledast h^*(-k,-\ell), \tag{78}$$

where $\circledast$ denotes convolution.

3) Generate a Gaussian white noise field G.
4) Generate the correlated Gaussian field X with correlation structure τ by applying the convolutional kernel h on the Gaussian white noise:

$$X = G \circledast h. \tag{79}$$

5) Generate the correlated uniform distribution field Y according to the ITM:

$$Y = F_X(X), \tag{80}$$

where F_X is the CDF of X.

6) Generate the correlated SAR image Z according to the ITM:

$$Z = F_Z^{-1}(Y), \tag{81}$$

where F_Z^{-1} is the estimated inverse CDF in the first step.

Figures 8–10 give simulation results for urban, forest, and wheat-growing areas, respectively. Figures 8(a)–10(a) present the generated SAR images for urban, forest, and wheat areas, respectively (left), and the corresponding original

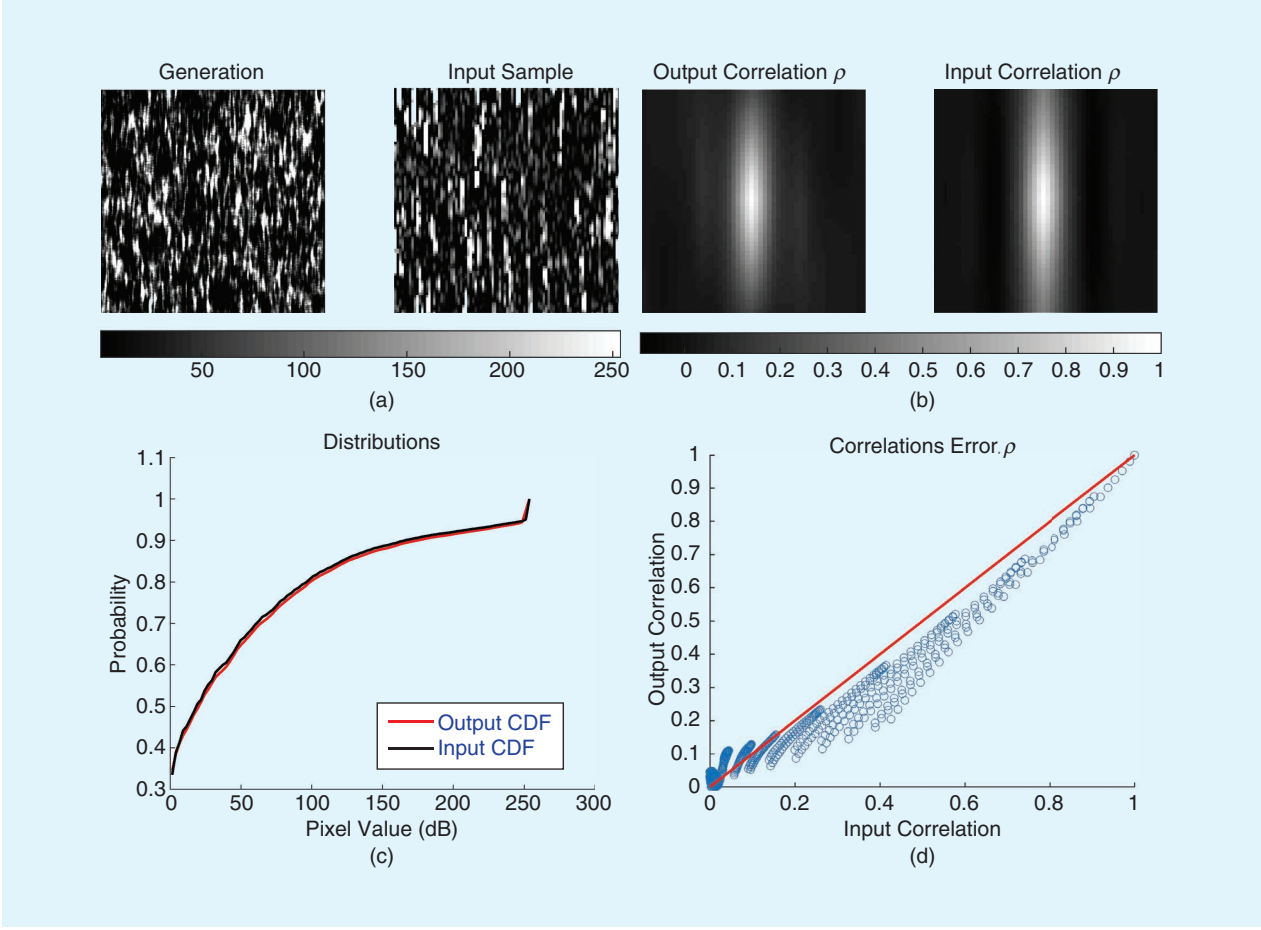

FIGURE 8. Simulation results for experimental SAR (E-SAR) data for urban areas. The (a) simulation results, (b) correlation structure, (c) CDF, and (d) correlation deviation.

input sample images (right). Figures 8(b)–10(b) illustrate the correlation structure ρ of the input sample (right) and the generated image (left). Figures 8(c)–10(c) show the marginal distributions of the input sample and the generated (output) images, respectively; black lines denote the CDF of the input sample, while the red line indicates the generated images. As expected, the CDFs are exactly matched. Figures 8(d)–10(d) convey the correlation deviation of the input sample image and the generated images. The horizontal axis is the correlation of the input sample, while the vertical axis is the correlation of the generated images; the closer the blue scatters are to the red 45° line, the smaller the deviation between the input correlation and generated correlation is. This approach produces slightly less-correlated samples.

Figure 11 presents the performance of the method for complex scenes using Flevoland AirSAR data with 15 identified terrain types [shown in Figure 11(e)]. Figure 11(a) indicates the original Flevoland AirSAR data, and Figure 11(d) depicts the ground truth of Flevoland, with the legend shown in Figure 11(e). The black frame in Figure 11(d) denotes the selected samples of each terrain type, which are used to generate SAR images. Figure 11(c) gives the generated results for Flevoland, which are based on the semantic map in Figure 11(b). Figure 11(b) contains the classification result from a convolutional neural network (CNN), which had an accuracy of 91% for 15 identified terrain types.

SIMULATION BASED ON THE COHERENT SCATTERER MODEL

The correlated clutter simulation methods introduced in the two previous sections replicate only the correlated clutter that satisfies the specific statistical distribution of SAR images, without considering the physical process of scattering. The computational SAR (cSAR) simulation system proposed by Allan et al. [27], [32], [36] starts from the statistical modeling of the underlying scatterers and simulates correlated *K*-distributed clutter based on the incoherent scatterer sum model. The incoherent scatterer sum model is degraded from the coherent scatterer model when neglecting the phase [1]. The cSAR system models the underlying scatterer as a correlated, gamma-distributed random field, and the position of the underlying scatterer is randomly distributed to obtain fully developed speckle. Then, correlated gamma-distributed RCS and correlated *K*-distributed SAR images are obtained. This system begins with the statistical characteristics of a single scatterer, instead of directly modeling the RCS σ. It aims to help explore the relationship between SAR image features and the underlying scatterer.

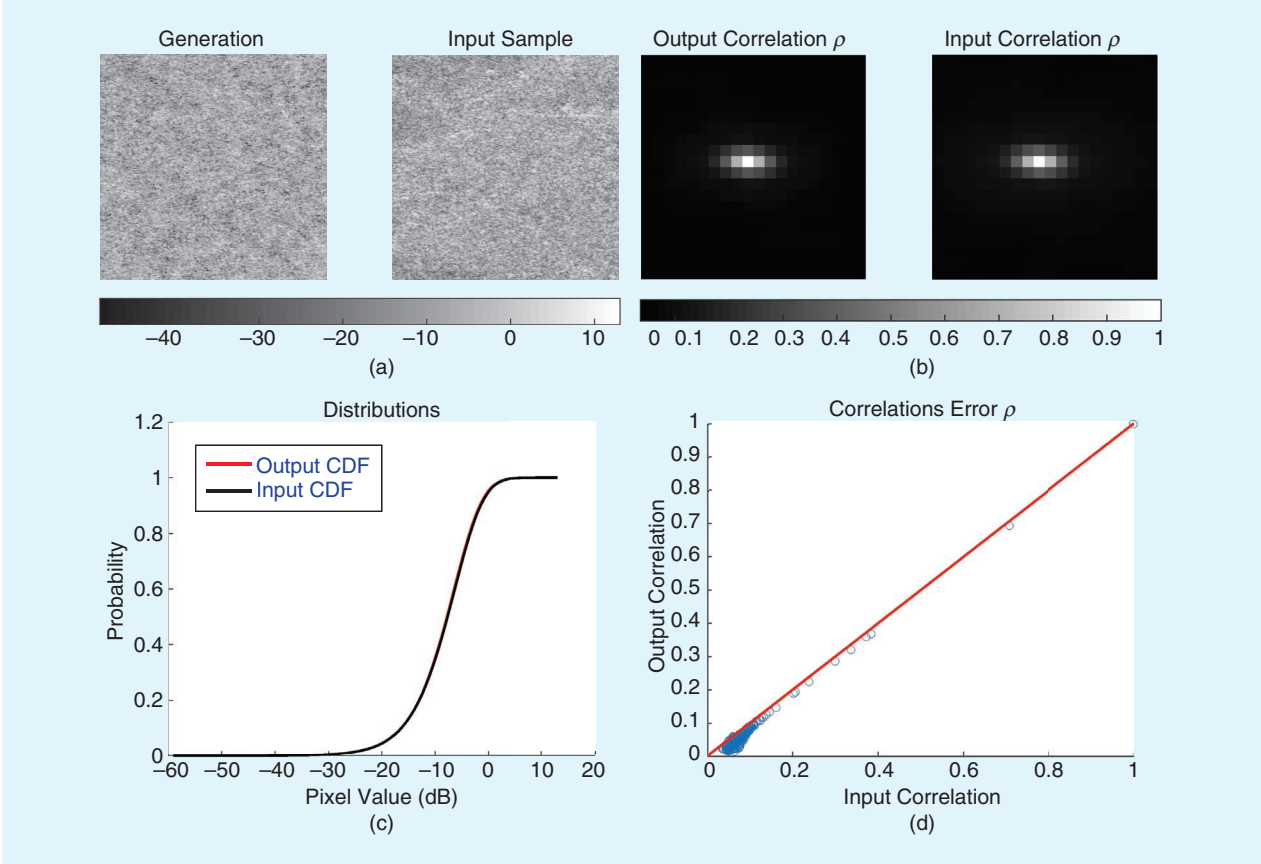

FIGURE 9. Simulation results for E-SAR data for forested areas. The (a) simulation results, (b) correlation structure, (c) CDF, and (d) correlation deviation.

Figure 12 illustrates the main simulation steps [27], [32], [36], which include the following:

1) Set randomly positioned scatterers. To produce fully developed speckle, there should be a large number of randomly distributed scatterers in each resolution cell. This is because the distance from the sensor to the target completely determines the phase of each scatterer and, if the range of the sensor covers many wavelengths, the scatterers with random locations will generate arbitrary phases. Therefore, during the simulation process, the ground coordinates (x, y) of the scatterer are uniformly distributed in the respective axial directions. This setting makes the number of scatterers N in each resolution cell obey a negative binomial distribution,

$$p(N; k, p) = \binom{k}{N} p^N (1-p)^{k-N}, \tag{82}$$

where k is the total number of Bernoulli trials and p is the probability of success in each trial. Here, k represents the total number of scatterers in the entire scene, and p is the ratio of the area of a resolution cell to the entire scene area. Usually, p is small.

2) Generate the correlated Gaussian random field G using the turning-bands method (TBM) [48]. Because the position of the underlying scatterer is random and cannot be represented by a regular grid, the correlated random field cannot be generated based on Fourier synthesis. Here, the TBM is used to generate irregularly distributed samples. It does not directly simulate the 2D random field but sums many 1D line processes that cross the field in random directions. As shown in Figure 13, the main process of simulating the scattered value $G(x_k, y_k)$ of the scatterer $P(x_k, y_k)$ at position (x_k, y_k) includes the following [36], [48]:

- Starting from an arbitrary origin O, M straight lines in random directions $\hat{u}_i$ are generated, and the angle between the ith line and the x-axis is denoted as θ_i.
- For the ith line, a random sample of the 1D random process Y_i with a zero mean and a correlation function $R_1(\xi_i)$ is generated, where ξ_i is the coordinate of the ith line.
- For each scatterer $P(x_k, y_k)$, $\vec{r}_k$ denotes the position vector at (x_k, y_k), and the coordinates of the projection of $\vec{r}_k$ onto the ith line with direction $\hat{u}_i$ is $\xi_{ik} = \vec{r}_k \cdot \hat{u}_i$. The corresponding value is $Y_i(\xi_{ik})$.
- Repeat steps 2 and 3 for all M lines to obtain the values $\{Y_i(\xi_{ik})\}, i = 1, 2, \ldots, M$.
- The scattered field $G(x_k, y_k)$ at position $P(x_k, y_k)$ can be obtained by addition and normalization:

$$G(x_k, y_k) = \frac{1}{\sqrt{M}} \sum_{i=1}^{M} Y_i(\vec{r}_k \cdot \hat{u}_i). \tag{83}$$

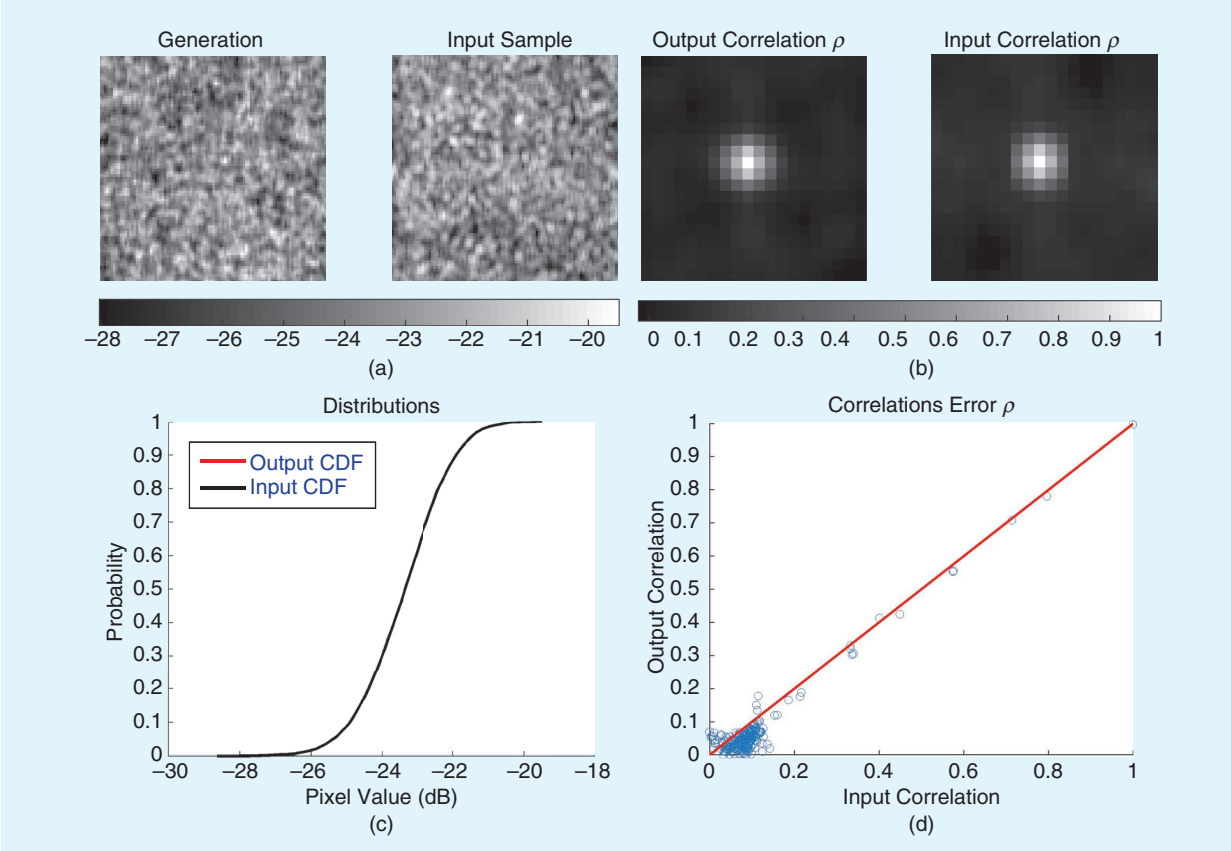

FIGURE 10. Simulation results for AirSAR data for wheat-growing areas. The (a) simulation results, (b) correlation structure, (c) CDF, and (d) correlation deviation.

The difficulty of the TBM is to establish a relationship between the correlation function $R_1(\xi_i)$ of the 1D linear process and the correlation function $R(x_1, x_2)$ of the desired 2D random field. Assuming that the implementation of Y_i in each line is independent of the others, the correlation function of the 2D field can be expressed as

$$R((x_1,y_1),(x_2,y_2)) = \langle G(x_1,y_1)G(x_2,y_2)\rangle = \frac{1}{M}\sum_{i=1}^{M}\langle Y_i(\vec{r}_1\cdot\hat{u}_i)Y_i(\vec{r}_2\cdot\hat{u}_i)\rangle. \quad (84)$$

If M is assumed to be large, e.g., of the order of 500, and $\hat{u}_i$ is uniformly distributed in the unit circle, $G(x_k, y_k)$ is a generalized stationary random field with the same correlation in all directions, and the preceding formula can be simplified as [36], [48]

$$R(r) = \frac{1}{2\pi}\int_{\text{unit circle}} R_1(\vec{h}\cdot\hat{u})\mathrm{d}\hat{u}, \quad (85)$$

where $\vec{h} = \vec{r}_2 - \vec{r}_1$. Therefore, it is necessary to obtain $R_1(\vec{h}\cdot\hat{u})$ based on the known $R(r)$ by inverting (85), which can be solved by the spectral representation method. If it is assumed that the 2D random field Z is isotropic, the radial spectral density function of the 2D random field is [48]

$$f(\omega) = \frac{\omega}{s^2}\int_0^{\infty} R(r)J_0(\omega r)r\mathrm{d}r, \quad (86)$$

where s^2 is the variance of the 2D random field and $J_0(\cdot)$ is the zero-order Bessel function of the first kind. The relationship between the radial spectral density function $f(\omega)$ of the 2D random field and the spectral density function $S_1(\omega)$ of the 1D line process is provided in [48]:

$$S_1(\omega) = \frac{s^2}{2}f(\omega). \quad (87)$$

For any given correlation function $R(r)$, $S_1(\omega)$ can be obtained by substituting the radial spectral density function $f(\omega)$ of the random field into (87). The method for generating 1D line processes is given in [49]:

$$Y_i(\vec{r}_k\cdot\hat{u}_i) = \sqrt{2}\cos(A_i\cdot(\vec{r}_k\cdot\hat{u}_i)+\Phi_i) = \sqrt{2}\cos(A_i(x_k\cos\theta_i + y_k\sin\theta_i)+\Phi_i), \quad (88)$$

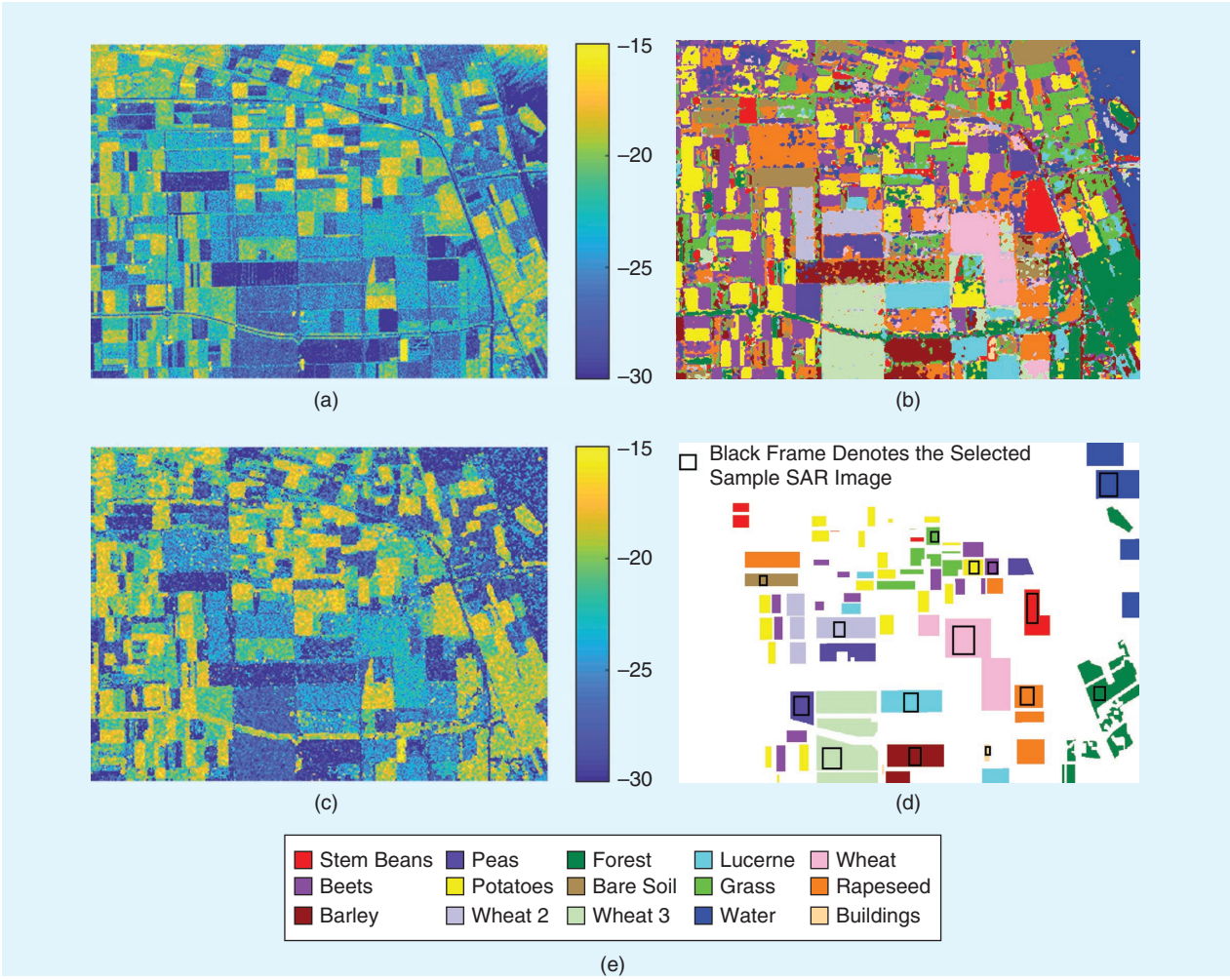

FIGURE 11. Simulation results for AirSAR data for Flevoland. The (a) Flevoland AirSAR data, (b) CNN classification result, (c) generated Flevoland data, and (d) selected samples. A legend for (b) and (d) appears in (e).

where Φ_i obeys a uniform distribution $\Phi_i \sim \mathcal{U}[0, \pi]$ and A_i is a random frequency following the probability density distribution $f(\omega)$. Finally, a 2D Gaussian random field with a correlation function of $R(r)$ can be obtained using (83). In addition, [50] points out that anisotropic 2D random fields can be approximated by the product of two mutually independent isotropic random fields.

3) Transform the correlated Gaussian random field into a correlated gamma-distributed random field Z using the MNLT method. The MNLT method [2], [13], [51] is employed to transform the correlated Gaussian random field into a gamma-distributed random field. It essentially equates variates of the Gaussian and gamma distributions at equivalent cumulative values, which brings

$$\frac{1}{\sqrt{2\pi}}\int_{-\infty}^{\gamma}\exp\left[-\frac{\gamma_0^2}{2}\right]d\gamma_0 \equiv \int_0^z \nu^{\nu}\frac{z_0^{\nu-1}}{\Gamma(\nu)}\exp[-\nu z_0]\mathrm{d}z_0. \quad (89)$$

The preceding equation defines the forward mapping function $\gamma = F(z)$ for $\gamma \to z$ and the inverse mapping function $z = F^{-1}(\gamma)$ for $\gamma_0 \leftarrow z$. Tough and Ward [52] gave the relationship between the autocorrelation coefficient $\rho_\gamma(r)$ of the Gaussian random field and the autocorrelation coefficient $\rho_z(r)$ of the gamma distribution as

$$\rho_z(r) = \frac{1}{\pi}\sum_{n=0}^{\infty}\frac{\rho_\gamma(r)^n}{2^n n!} \times\left(\int_{-\infty}^{\infty}\exp(-x^2)H_n(x)Q_z\left(\frac{\mathrm{erfc}(x)}{2}\right)\mathrm{d}x\right)^2, \quad (90)$$

where $H_n(\cdot)$ is the Hermite polynomial defined by

$$H_n(z) = (-1)^n\exp(z^2)\frac{d^n}{dz^n}\exp(-z^2), \quad (91)$$

$\mathrm{erfc}(x)$ is the error function defined by

$$\mathrm{erfc}(x) = \frac{2}{\sqrt{\pi}}\int_0^x e^{-\eta^2}d\eta, \quad (92)$$

and $Q_z(\varsigma)$ is the complementary quantile function of the gamma distribution, which is defined as

$$\int_{Q_z(\varsigma)}^{\infty} p(z)\mathrm{d}z = \varsigma, \quad (93)$$

where $p(z)$ is the PDF of the gamma distribution. This is, essentially, the inversion method instantiated for the gamma distribution.

4) Generate RCS σ based on an LSP [53]. The scattered field of the underlying scatterer that obeys a correlated gamma distribution in the previous steps has been obtained. Now, RCS σ can be determined according to the incoherent scatterer sum model (41) (see the "Fluctuation of a Single Scatterer" section), which can be regarded as an LSP, an incoherent summation of the underlying scatterers in a resolution cell. The size of the LSP windows is chosen to match the –3-dB resolution, which is an approximation to the real RCS. The RCS is regarded as a correlated gamma-distributed random field by adopting the approximation validated by Kotz and Neumann [34], which assumes that the sum of correlated gamma variables can be approximately described by a gamma distribution. The parameters of the RCS can be estimated by the maximum likelihood [32]. The correlation coefficient relationship caused by an LSP has been shown

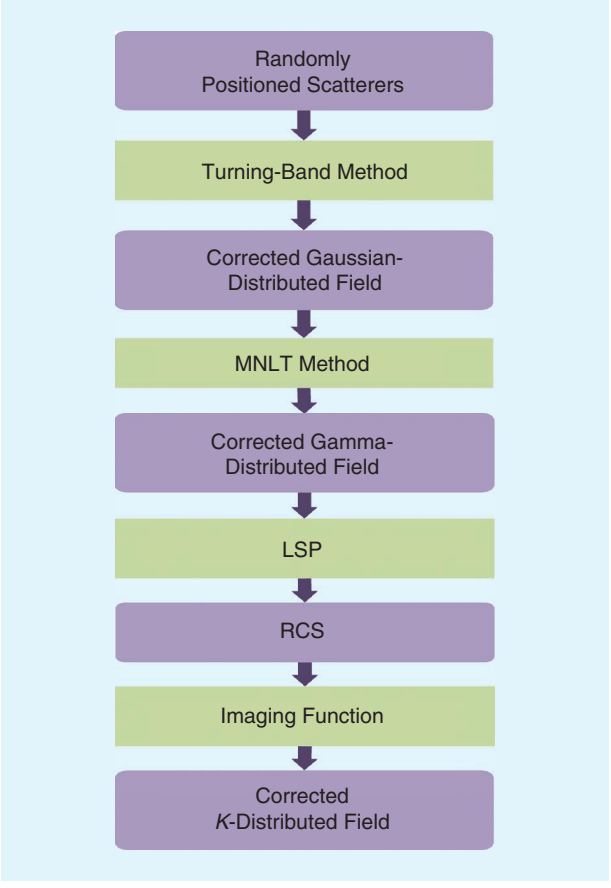

FIGURE 12. A correlated clutter simulation based on the coherent scatterer model.

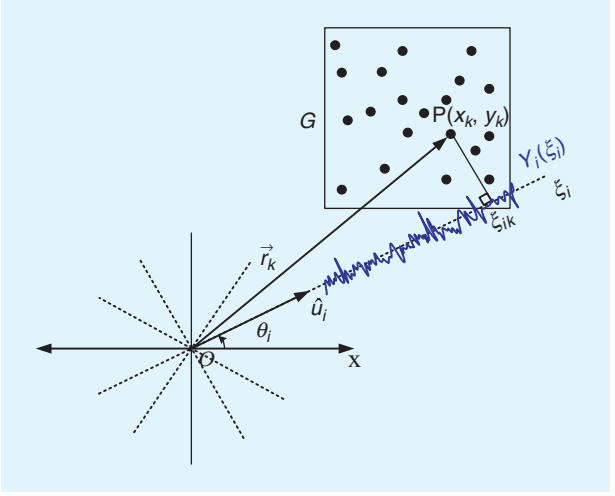

FIGURE 13. The TBM.

in (43) in the "Fluctuation of a Single Scatterer" section.

5) Obtain the correlated *K*-distributed clutter image through the imaging system. As introduced earlier, given the parameters of the density of the scatterer, the order of the gamma distribution, and the desired correlation information, the TBM is first used to simulate the correlated Gaussian random field, and the MNLT technique is employed to convert to the correlated gamma-distributed random field. Thereafter, the RCS that obeys the correlated gamma distribution is obtained through the LSP. Finally, the single-look complex image can be generated by inputting the RCS into the imaging system through a simple range Doppler algorithm. The correlated intensity image that obeys the *K* distribution is the squared envelope of the single-look complex image [32]. The entire process is implemented based on the Monte Carlo method.

The simulation results following the preceding steps can be found in [27], [32], and [36]. This simulation method can be used to explore the relationship between SAR image characteristics and the physical scattering process, which is a better representation for SAR imagery. Its extension and application will be more in line with real-world modeling.

SIMULATION BASED ON THE GGCS

Yue et al. [38] recently proposed a GGCS model for correlated SAR clutter simulation. The GGCS model can be seen as a simplification of the coherent scatterer model, which assumes that the scattered field of a single scatterer in a resolution cell is complex Gaussian distributed. It is physics plausible and can be used to simulate the correlated SAR clutter of various scenarios. The authors proved that this approach was able to represent a large variety of single-point probability distribution models commonly used in the literature. The correlation information of SAR images is introduced by the spatial correlation structures in the complex Gaussian field of a single scatterer in a resolution cell and in the number of scatterers. The theoretical relationship of the distribution parameters and the correlation coefficient between the SAR image and the complex Gaussian field was derived in [38], which guided the correlated clutter simulation.

The main simulation process is described in Figure. 14. The input is an image sample, from which one selects the single-pixel distribution model and estimates the model's parameters as well as the correlation structure. With this information, and using the theoretical relationships presented in [38], one obtains the distribution parameters of the complex Gaussian field scattered by a single scatterer and of the number of scatterers for the generalized model. The correlation coefficients of the Gaussian field and the number of scatterers are also determined by the correlation coefficient of the real component and the intensity SAR data, according to the relationships

$$\rho_{\Re\Re}(\tau)=\frac{\langle \min\{N(0),N(\tau)\}\rangle}{\mu_N}\langle \rho_{xx}(i,\tau)\rangle, \tag{94}$$

$$\rho_{II}(\tau)=\frac{\langle N_m N_m\rangle \rho_{xx}^2(\tau)+\rho_{NN}(\tau)\sigma_N^2}{2\sigma_N^2+\mu_N^2}, \tag{95}$$

where $\rho_{xx}(i,\tau)$, $\rho_{NN}(\tau)$, $\rho_{\Re\Re}(\tau)$, and $\rho_{II}(\tau)$ are correlation coefficients of the complex Gaussian field, the number of scatterers, the real component, and the intensity SAR data, respectively; μ_N and σ_N^2 are the mean and the variance of the number of scatterers N, respectively; $N(0)$ denotes the number of scatterers at the current position; $N(\tau)$ is the number of scatterers at distance τ; and $N_m=\min[N(0),N(\tau)]$.

The corresponding convolution kernels are obtained according to (78), which can be implemented by a Fourier transform. Finally, given 1) the distribution parameters of the complex Gaussian field, 2) the distribution parameters of the number of scatterers, and 3) the convolution kernels, the generalized model can be used to obtain data with the same marginal distribution and correlation structure as the input sample. Figures 15 and 16 show simulation results based on the GGCS model. The model performs well on most sea and vegetated clutters (farmland and forests).

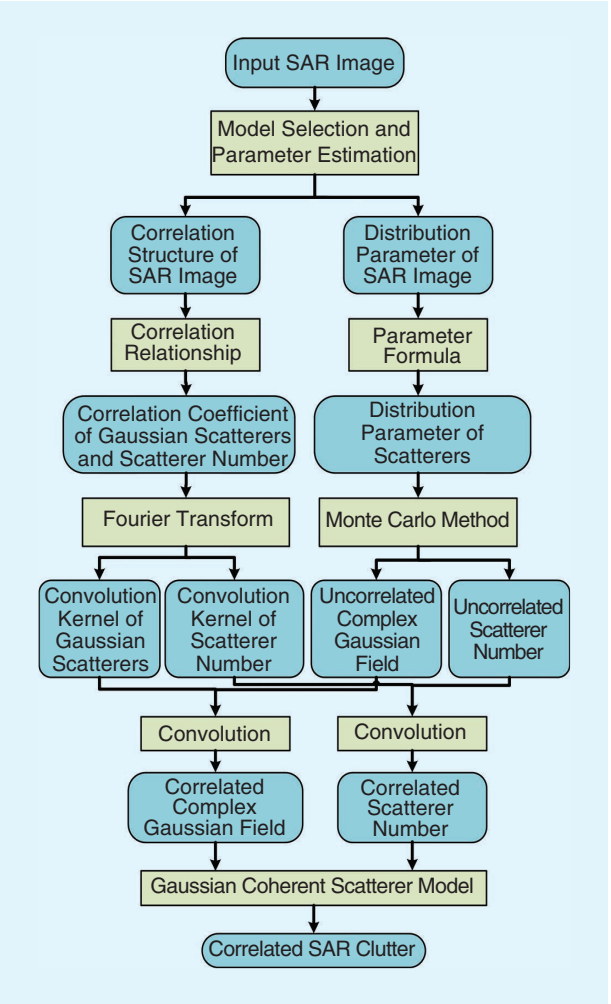

FIGURE 14. A correlated clutter simulation based on the GGCS model.

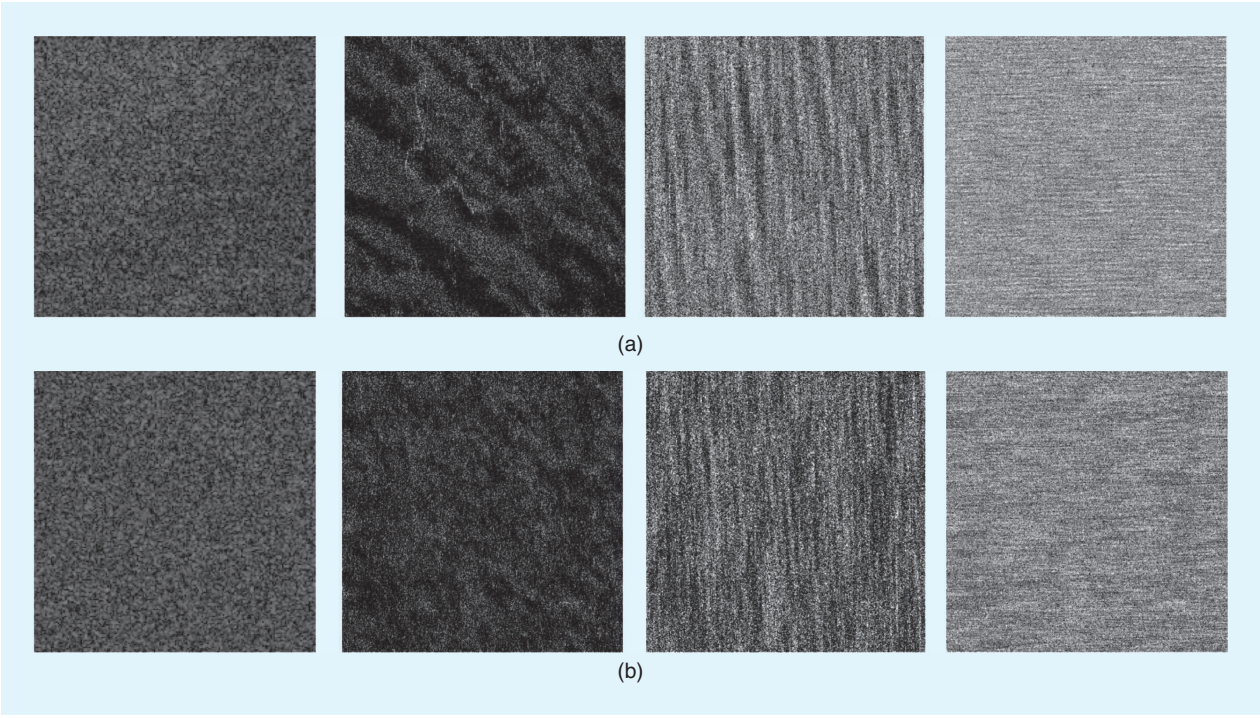

FIGURE 15. A comparison of (a) an actual SAR clutter and (b) a simulated SAR clutter of various scenarios based on the GGCS model. From left to right: sea 1, sea 2, sea 3, and sea 4.

However, it fails to capture the deterministic patterns, such as urban locales and mountainous areas, which is expected, as the GGCS model itself is only for stationary stochastic fields. The authors of [38] discuss this issue in detail.

CONCLUSIONS

This article reviewed spatial correlation analysis and correlated clutter simulation for SAR images, based on [1]. It summarized the two main approaches for simulating spatial correlation: one based on the product model and another founded on the coherent scatterer model. The former is relatively simple and easy to analyze, but it characterizes only the correlation characteristics of the image itself since it does not involve physical processes, and it does not support a systematic understanding of SAR images. The latter starts from the physical modeling of the underlying scatterers and considers the effect of the number of scatterers, the bottom scatterer, and the imaging function on the spatial correlation of the observed image based on the imaging process. The analysis of the latter is more sophisticated, as it involves complicated derivations, but it can explain the correlation characteristics of the images from the fundamental scattering process, which is helpful for a deep understanding of SAR images. With the acquisition of high-resolution and ultrahigh-resolution images, more and more physical information is contained, and it is important to analyze the main factors that lead to the correlation data in SAR images, such as the spatial resolution, sampling interval, and size of features. In this case, a more refined correlation model is necessary, and the advantage of correlation analysis based on the coherent scatterer models becomes apparent.

For the correlated clutter simulation problem, four correlated clutter simulation methods based on two classical distributions, namely, K and G^0, have been summarized: a product model-based method, an ITM-based approach, a coherent scatterer model-based technique, and the GGCS approach. The first two techniques are directly based on the statistical characteristics of an image. The latter two start from the modeling of the underlying scatterers and build the statistical relationship between the underlying scatterers and the received correlated clutter image. This kind of physics-based model shows better development prospects in today's high-resolution SAR image applications. In addition, the existing statistical modeling of SAR images mainly describes clutter textures, disregarding the boundary and contour information, which is far from sufficient for SAR image analysis of complex scenes. Therefore, it is an important direction to enhance the semantic information of the scene and explore SAR image simulation under the comprehensive influence of high-level semantics and the underlying coherent scattering process.

ACKNOWLEDGMENT

This work was supported, in part, by the Natural Science Foundation of China, under grants 61991422 and 61822107. The authors would like to thank Jing-Jing Zhang of the Institute of Electronics, Chinese Academy of Sciences for providing the E-SAR data acquired over Traunstein, Germany.

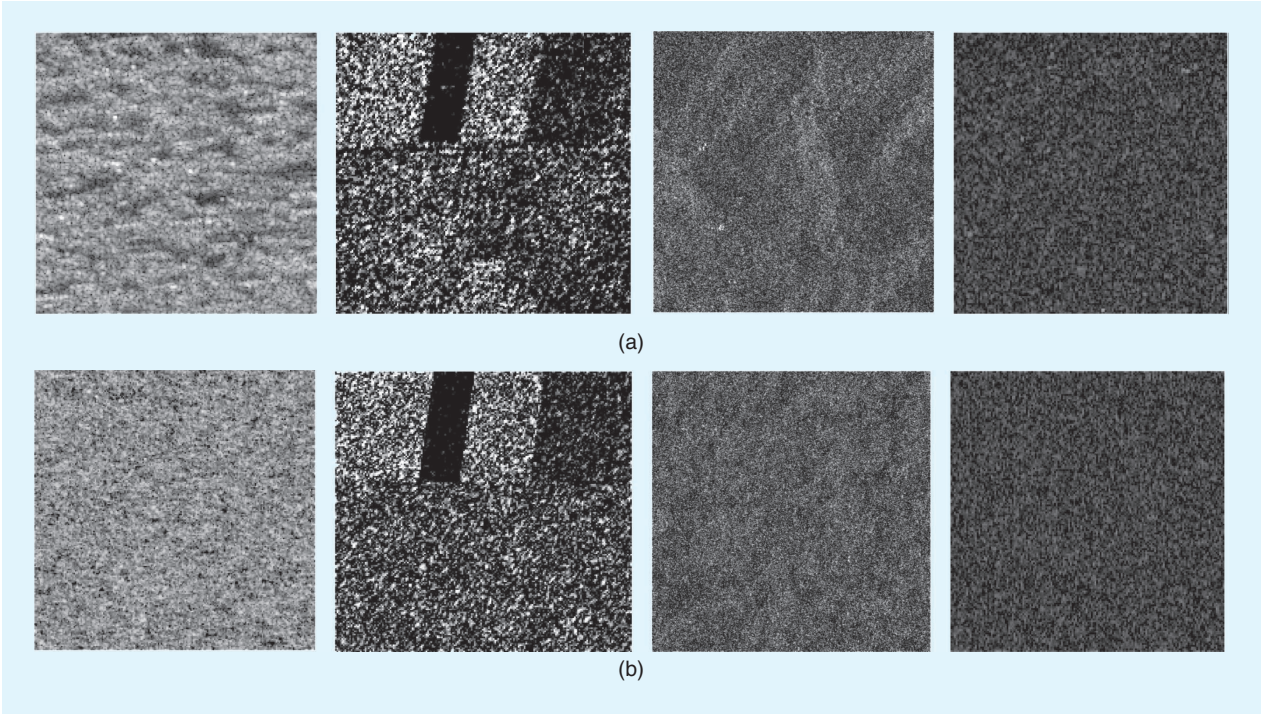

FIGURE 16. A comparison of (a) an actual SAR clutter and (b) a simulated SAR clutter of various scenarios based on the GGCS model. From left to right: urban, farmland, forest 2, and road images.

AUTHOR INFORMATION

Dong-Xiao Yue (dxyue15@ fudan.edu.cn) received her B.E. degree in communication engineering from Nanjing University of Posts and Telecommunications, China, in 2015 and the Ph.D. degree in electromagnetic field and microwave technology from Fudan University, Shanghai, China, in 2020. She is currently with the College of Information Engineering, Shanghai Maritime University. Her research interests include statistical analysis for SAR images, Bayesian inversion methods, and deep learning. She is a Student Member of IEEE.

Feng Xu (fengxu@fudan.edu.cn) received his B.E. degree with honors in information engineering from Southeast University, Nanjing, China, and his Ph.D. degree with honors in electronic engineering from Fudan University, Shanghai, China, in 2003 and 2008, respectively. He is a professor with Fudan University and serves as vice dean of the School of Information Science and Technology and vice director of the MoE Key Lab for Information Science of Electromagnetic Waves. Among other honors, he was awarded the second-place National Nature Science Award of China in 2011. He was the 2014 recipient of the Early Career Award of the IEEE Geoscience and Remote Sensing Society (GRSS) and the 2007 recipient of the SUMMA graduate fellowship in the area of advanced electromagnetics. He currently serves as associate editor for *IEEE Geoscience and Remote Sensing Letters*. He is the founding chair of the IEEE GRSS Shanghai Chapter. He is a Senior Member of IEEE.

Alejandro C. Frery (alejandro.frery@vuw.ac.nz) received his B.Sc. degree in electronic and electrical engineering from the Universidad de Mendoza, Argentina, in 1985, his M.Sc. degree in applied mathematics (statistics) from the Instituto de Matemática Pura e Aplicada (IMPA), Rio de Janeiro, Brazil, in 1990, and his Ph.D. degree in applied computing from the Instituto Nacional de Pesquisas Espaciais (INPE), São José dos Campos, Brazil, in 1993. He is the founder of the Laboratório de Computação Científica e Análise Numérica, Universidade Federal de Alagoas, Maceió, Brazil. He is a Huashan Scholar with Xiamen University, Xi'an, China. His research interests include stochastic modeling and computational statistics. He is currently with the School of Mathematics and Statistics, Victoria University of Wellington, New Zealand. He is a Senior Member of IEEE.

Ya-Qiu Jin (yqjin@fudan.edu.cn) received his bachelor's degree in electrical engineering from Peking University, Beijing, China, in 1970 and his M.S., E.E., and Ph.D. degrees in computer science from the Massachusetts Institute of Technology, Cambridge, in 1982, 1983, and 1985, respectively. He is currently the Academician of the Chinese Academy of Sciences. Among other honors, he received the first-grade MoE Science Prize in 1992, 1996, and 2009; the first-grade Guanghua Science Prize in 1993; the IEEE Geoscience and Remote Sensing Society (GRSS) Award in 2010; the China National Science Prize in 1993 and 2011; the Shanghai Sci/Tech Gong Cheng Award in 2015; and the IEEE GRSS Distinguished Achievement Award in 2015. He was the general cochair of IGARSS 2016 in Beijing and an associate editor of *IEEE Transactions on Geoscience and Remote Sensing* from 2005 to 2012. He is an IEEE Life Fellow.

REFERENCES

[1] D.-X. Yue, F. Xu, A. C. Frery, and Y.-Q. Jin, "SAR image statistically modeling part I: Single-pixel models," *IEEE Geosci. Remote Sens. Mag.*, early access, 2019. doi: 10.1109/MGRS.2020.3004508.

[2] C. Oliver and S. Quegan, *Understanding Synthetic Aperture Radar Images*. Raleigh, NC: SciTech, 2004.

[3] E. Jakeman and P. N. Pusey, "A model for non-Rayleigh sea echo," *IEEE Trans. Antennas Propag.*, vol. 24, no. 6, pp. 806–814, 1976. doi: 10.1109/TAP.1976.1141451.

[4] E. Jakeman, "On the statistics of K-distributed noise," *J. Phys. A, Math. Gen.*, vol. 13, no. 1, pp. 31–48, 1980. doi: 10.1088/0305-4470/13/1/006.

[5] E. Jakeman and R. J. A. Tough, "Non-Gaussian models for the statistics of scattered waves," *Adv. Phys.*, vol. 37, no. 5, pp. 471–529, 1988. doi: 10.1080/00018738800101419.

[6] C. J. Oliver, "A model for non-Rayleigh scattering statistics," *Opt. Acta Int. J. Opt.*, vol. 31, no. 6, pp. 701–722, 1984. doi: 10.1080/713821561.

[7] C. J. Oliver, "Correlated K-distributed clutter models," *Opt. Acta Int. J. Opt.*, vol. 32, no. 12, pp. 1515–1547, 1985. doi: 10.1080/713821683.

[8] C. J. Oliver and R. J. A. Tough, "On the simulation of correlated K-distributed random clutter," *Opt. Acta Int. J. Opt.*, vol. 33, no. 3, pp. 223–250, 1986. doi: 10.1080/713821938.

[9] C. J. Oliver, "The interpretation and simulation of clutter textures in coherent images," *Inverse Problems*, vol. 2, no. 4, pp. 481–518, 1986. doi: 10.1088/0266-5611/2/4/012.

[10] E. Jakeman, "Statistics of integrated gamma-lorentzian intensity fluctuations," *Opt. Acta Int. J. Opt.*, vol. 27, no. 6, pp. 735–741, 1980. doi: 10.1080/713820299.

[11] R. J. A. Tough, "A Fokker-Planck description of K-distributed noise," *J. Phys. A, Gen. Phys.*, vol. 20, no. 3, pp. 551–567, 1987. doi: 10.1088/0305-4470/20/3/017.

[12] C. J. Oliver, "On the simulation of coherent clutter textures with arbitrary spectra," *Inverse Problems*, vol. 3, no. 3, pp. 463–475, 1987. doi: 10.1088/0266-5611/3/3/014.

[13] K. D. Ward, R. J. A. Tough, and S. Watts, "Sea clutter: Scattering, the K distribution and radar performance," *Waves Random Complex Media*, vol. 17, no. 2, pp. 233–234, 2013. doi: 10.1080/17455030601097927.

[14] A. P. Blake, D. Blacknell, and C. J. Oliver, "Texture simulation and analysis in coherent imagery," presented at the 5th Int. Conf. Image Process. Appl., Edinburgh, 1995, pp. 772–776. doi: 10.1049/cp:19950764.

[15] E. Conte, G. Galati, and M. Longo, "Exogenous modelling of non-Gaussian clutter," *J. Inst. Electron. Radio Eng.*, vol. 57, no. 4, pp. 151–155, 1987. doi: 10.1049/jiere.1987.0056.

[16] E. Conte, M. D. Bisceglie, M. Lops, and G. Ricci, "Simulation of correlated random fields with gamma-distributed amplitude for SAR applications," in *Proc. IEEE Geosci. Remote Sens. Symp.*, 1991, pp. 2397–2400.

[17] E. Conte, M. Longo, and M. Lops, "Modeling and simulation of non-Rayleigh radar clutter," *IEE Proc. F, Radar Signal Process.*, vol. 138, no. 2, pp. 121–130, 1991. doi: 10.1049/ip-f-2.1991.0018.

[18] E. Conte and M. Longo, "Characterisation of radar clutter as a spherically invariant random process," *IEE Proc. F, Radar Signal Process.*, vol. 134, no. 2, pp. 191–197, 1987. doi: 10.1049/ip-f-1.1987.0035.

[19] K. D. Ward, "Compound representation of high resolution sea clutter," *Electron. Lett.*, vol. 17, no. 16, pp. 561–563, 1981. doi: 10.1049/el:19810394.

[20] F. T. Ulaby, F. Kouyate, B. Brisco, and T. H. L. Williams, "Textural information in SAR images," *IEEE Trans. Geosci. Remote Sens.*, vol. GE-24, no. 2, pp. 235–245, 1986. doi: 10.1109/TGRS.1986.289643.

[21] R. Touzi, "A review of speckle filtering in the context of estimation Theory," *IEEE Trans. Geosci. Remote Sens.*, vol. 40, no. 11, pp. 2392–2404, 2002. doi: 10.1109/TGRS.2002.803727.

[22] J. S. Lee, "Speckle analysis and smoothing of synthetic aperture radar images," *Comput. Graph. Image Process.*, vol. 17, no. 1, pp. 24–32, 1981. doi: 10.1016/S0146-664X(81)80005-6.

[23] G. Margarit, J. J. Mallorqui, J. M. Rius, and J. Sanz-Marcos, "On the usage of GRECOSAR, an orbital polarimetric SAR simulator of complex targets, to vessel classification studies," *IEEE Trans. Geosci. Remote Sens.*, vol. 44, no. 12, pp. 3517–3526, 2006. doi: 10.1109/TGRS.2006.881120.

[24] Y. Cheng et al., "Monitoring of oil spill trajectories with COSMO-SkyMed X-band SAR images and model simulation," *IEEE J. Sel. Topics Appl. Earth Observ. Remote Sens.*, vol. 7, no. 7, pp. 2895–2901, 2014. doi: 10.1109/JSTARS.2014.2341574.

[25] S. Auer, I. Hornig, M. Schmitt, and P. Reinartz, "Simulation-based interpretation and alignment of high-resolution optical and SAR images," *IEEE J. Sel. Topics Appl. Earth Observ. Remote Sens.*, vol. 10, no. 11, pp. 4779–4793, 2017. doi: 10.1109/JSTARS.2017.2723082.

[26] J. Tao, S. Auer, G. Palubinskas, P. Reinartz, and R. Bamler, "Automatic SAR simulation technique for object identification in complex urban scenarios," *IEEE J. Sel. Topics Appl. Earth Observ. Remote Sens.*, vol. 7, no. 3, pp. 994–1003, 2014. doi: 10.1109/JSTARS.2013.2275928.

[27] J. M. Allan, M. J. Collins, and C. Gierull, "Computational synthetic aperture radar (cSAR): A flexible signal simulator for multichannel SAR systems," *Can. J. Remote Sens.*, vol. 36, no. 4, pp. 345–360, 2010. doi: 10.5589/m10-048.

[28] J. B. Billingsley, A. Farina, F. Gini, M. V. Greco, and L. Verrazzani, "Statistical analyses of measured radar ground clutter data," *IEEE Trans. Aerosp. Electron. Syst.*, vol. 35, no. 2, pp. 579–593, 1999. doi: 10.1109/7.766939.

[29] G. Gui, "Statistical modeling of SAR images: A survey," *Sensors*, vol. 10, no. 1, pp. 775–795, 2010. doi: 10.3390/s100100775.

[30] O. H. Bustos, A. G. Flesia, A. C. Frery, and M. M. Lucini, "Simulation of spatially correlated clutter fields," *Commun. Statist., Simul. Comput.*, vol. 38, no. 10, pp. 2134–2151, 2009. doi: 10.1080/03610910903249536.

[31] A. C. Frery, H. J. Muller, C. C. F. Yanasse, and S. J. S. Sant'Anna, "A model for extremely heterogeneous clutter," *IEEE Trans. Geosci. Remote Sens.*, vol. 35, no. 3, pp. 648–659, 1997. doi: 10.1109/36.581981.

[32] M. J. Collins and J. M. Allan, "Modeling and simulation of SAR image texture," *IEEE Trans. Geosci. Remote Sens.*, vol. 47, no. 10, pp. 3530–3546, 2009. doi: 10.1109/TGRS.2009.2021260.

[33] R. J. A. Tough, "A Fokker-Planck description of K-distributed noise," *J. Phys. A, Gen. Phys.*, vol. 20, no. 3, p. 551, 1999. doi: 10.1088/0305-4470/20/3/017.

[34] S. Kotz and J. Neumann, "On the distribution of precipitation amounts for periods of increasing length," *J. Geophys. Res.*, vol. 69, no. 4, pp. 800–801, 1963. doi: 10.1029/JZ069i004p00800.

[35] K. J. W. Adams, "Distribution of sum of identically distributed exponentially correlated gamma-variables," *Ann. Math. Statist.*, vol. 35, no. 1, pp. 277–283, 1964. doi: 10.1214/aoms/1177703750.

[36] J. M. Allan, "Design and testing of a SAR simulation system," M.S. thesis, Dept. of Elect. and Comput. Eng., Univ. of Calgary, Calgary, Canada, 2006.

[37] O. H. Bustos, A. G. Flesia, and A. C. Frery, "Generalized Method for Sampling Spatially Correlated Heterogeneous Speckled Imagery," *EURASIP J. Adv. Signal Process.*, vol. 2001, no. 2, pp. 1–11, 2001. doi: 10.1155/S1110865701000166.

[38] D.-X. Yue, F. Xu, A. C. Frery, and Y.-Q. Jin, "A generalized Gaussian coherent scatterer model for correlated SAR texture," *IEEE Trans. Geosci. Remote Sens.*, vol. 58, no. 4, pp. 2947–2964, 2020. doi: 10.1109/TGRS.2019.2958125.

[39] D. Chan, A. Rey, J. Gambini, and A. C. Frery, "Sampling from the GI0 Distribution," *Monte Carlo Methods Appl.*, vol. 24, no. 4, pp. 271–287, 2018. doi: 10.1515/mcma-2018-2023.

[40] D. Blacknell, "New method for the simulation of correlated K-distributed clutter," *IEE Proc., Radar, Sonar Navig.*, vol. 141, no. 1, pp. 53–58, 1994. doi: 10.1049/ip-rsn:19949706.

[41] B. C. Armstrong and H. D. Griffiths, "Modelling spatially correlated K-distributed clutter," *Electron. Lett.*, vol. 27, no. 15, pp. 1355–1356, 1991. doi: 10.1049/el:19910853.

[42] M. B. Sechtin, L. M. Novak, and M. C. Burl, "Algorithms for optimal processing of polarimetric radar data," MIT-Lincoln Lab., Lexington, MA, Project Rep. TT-73, 1989.

[43] A. Papoulis and S. U. Pillai, *Probability, Random Variables, and Stochastic Processes*, 4th ed. New York: McGraw-Hill, 2002.

[44] M. Abramowitz, I. A. Stegun, and J. E. Romain, *Handbook of Mathematical Functions, with Formulas, Graphs, and Mathematical Tables*. New York: Dover, 1970.

[45] Z. X. Wang and T. R. Guo, *Introduction to Special Functions*. Beijing: Science Press, 1979.

[46] R. J. A. Tough and K. D. Ward, "The generation of correlation K-distribution noise," DRA, Malvern, U.K., DRA Tech. Rep. DRA/CIS/CBC3/WP94001/2.0, 1994.

[47] D.-X. Yue, F. Xu, A. C. Frery, and Y.-Q. Jin, "SAR image generation with semantic-statistical convolution," presented at the IEEE Int. Geosci. Remote Sens. Symp. (IGARSS), Yokohama, Japan, 2019, pp. 9999–10,002. doi: 10.1109/IGARSS.2019.8900225.

[48] A. Mantoglou and J. L. Wilson, "The Turning Bands method for simulation of random fields using line generation by a spectral method," *Water Resour. Res.*, vol. 18, no. 5, pp. 1379–1394, 1982. doi: 10.1029/WR018i005p01379.

[49] M. Schlather, "Introduction to positive definite functions and to unconditional simulation of random fields," Dept. of Mathematics and Statistics, Lancaster University, Lancaster, U.K., Tech. Rep. ST-99-10, 1999.

[50] C. R. Dietrich, "A simple and efficient space domain implementation of the turning bands method," *Water Resour. Res.*, vol. 31, no. 1, pp. 147–156, 1995. doi: 10.1029/94WR01457.

[51] K. D. Ward, R. J. A. Tough, and P. W. Shepherd, "Modelling sea clutter: Correlation, resolution and non-Gaussian statistics," in *Proc. Radar 97*, 1997, pp. 95–99. doi: 10.1049/cp:19971639.

[52] R. J. A. Tough and K. D. Ward, "The correlation properties of gamma and other non-Gaussian processes generated by memoryless nonlinear transformation," *J. Phys. D, Appl. Phys.*, vol. 32, no. 23, pp. 3075–3084, 1999. doi: 10.1088/0022-3727/32/23/314.

[53] E. Vanmarcke, *Random Fields: Analysis and Synthesis*. Cambridge, MA: MIT Press, 1988.

GRS